https://doi.org/10.5194/egusphere-2025-6336
Preprint. Discussion started: 19 January 2026

Influence of Ni-related enzymes on the Ni cycle in the Southern Ocean: insights from isotopes and metagenomics

Nolwenn Lemaitre[1,2*], Emile Faure[3,4*], Ricardo Zamora[2], Corey Archer[2], Matthias Sieber[2,5], Michael Ellwood[6], Christel Hassler[7,8], Yajuan Lin[9,10,11], Nicolas Cassar[10,11], Lois Maignien[4,12], Derek Vance[2]

[1]LEGOS (CNRS/CNES/IRD/UT3), University of Toulouse, Toulouse, FR-31400, France
[2]Department of Earth and Planetary Sciences, Institute of Geochemistry and Petrology, ETH Zurich, Zurich, CH-8092, Switzerland
[3]Station Biologique de Roscoff, CNRS/Sorbonne University, Roscoff, FR-29680, France
[4]Univ Brest, CNRS, IFREMER, BEEP, Plouzané, FR-29280, France
[5]College of Marine Science, University of South Florida, St. Petersburg, FL-33701, USA
[6]Research School of Earth Sciences, Australian National University, Canberra, ACT-2601, Australia
[7]Institute of Earth Sciences, University of Lausanne, Lausanne, CH-1015, Switzerland
[8]School of Architecture, Civil & Environmental Engineering, Alpine and Polar Environmental Research Center, EPFL, Sion, CH-1951, Switzerland
[9]Department of Life Sciences, Texas A&M University Corpus Christi, Corpus Christi, TX-78412, USA
[10]Division of Earth and Climate Sciences, Nicholas School of the Environment, Duke University, Durham, NC-27708, USA
[11]CNRS, Univ Brest, IRD, Ifremer, LEMAR, Plouzané, FR-29280, France
[12]Bay Paul Center, Marine Biological Laboratory, Woods Hole, MA-02543, USA

Correspondence to: Nolwenn Lemaitre (nol.lemaitre@gmail.com) and Emile Faure (emile.faure@sb-roscoff.fr)
*These authors contributed equally to this work.

Abstract. Nickel (Ni) is an essential micronutrient for marine microorganisms, being involved in enzymes controlling the nitrogen cycle and metabolic responses to oxidative stress. In this study, we examine the covariation between the abundance of Ni-related enzymes and Ni isotope fractionation. To do so, dissolved Ni concentrations and isotope compositions are presented together with metagenomics on samples from the Antarctic Circumnavigation Expedition. Overall, results reveal lower Ni concentrations and higher δ^{60}Ni values in surface waters north of the Sub-Antarctic Front compared to southerly stations. One exception is seen near the high-latitude Mertz Glacier, where the systematics between Ni and δ^{60}Ni better resemble those of low-latitude stations. Relative abundances of urease and Ni-SOD in metagenomes are found to correlate with δ^{60}Ni, potentially suggesting preferential biological uptake of Ni by the organisms using these enzymes. We find a particularly high abundance of urease in diatoms and alphaproteobacteria near the Mertz Glacier, matching the surprisingly high δ^{60}Ni. We thus hypothesise that urea could serve as a nitrogen source for microbial organisms in the late stage of polynya diatom blooms, perhaps causing the observed Ni drawdown and isotope fractionation. This study represents an initial exploration of the influence of biological processes on Ni and δ^{60}Ni distributions. It constitutes a first step towards the further analyses (*e.g.*, culture experiments and metatranscriptomics) needed to determine which exact processes lead to the δ^{60}Ni biogeochemical divide observed between low-latitude and high-latitude waters.

https://doi.org/10.5194/egusphere-2025-6336
Preprint. Discussion started: 19 January 2026

1 Introduction

The biogeochemical cycling of nutrients in the ocean is controlled by microbial organisms. Typically nutrient concentrations are drawn down in surface waters associated with phytoplankton utilisation, and released at depth due to remineralisation by heterotrophic bacteria. These key biological reactions are mediated by enzymes, most of which contain transition metals (Morel et al., 2020). Among these different enzymatic roles, Ni is required as the metallocenter for the 'urease' enzyme that recycles urea back to bioavailable ammonia, the 'NiFe hydrogenase' enzyme that oxidises dihydrogen produced during nitrogen fixation, and the 'Ni superoxide dismutase' (Ni-SOD) enzyme that degrades superoxide radicals and other reactive oxygen species generated through photosynthesis and respiration (Ragsdale, 2009). Although different isoforms of the SOD enzyme are observed (including those with Mn, Fe, Cu or Zn in the metal active site), only the Ni-SOD is found in different types of cyanobacteria (*Prochlorococcus*, most *Synechococcus*, a few *Trichodesmium* species), in heterotrophic bacteria, and in the picoeukaryote *Ostreococcus* (Dupont et al., 2008b, 2010). These enzymatic roles have been evidenced by controlled culture experiments involving Ni amendments. Diatoms respond to Ni addition when grown only on urea as a nitrogen source, illustrating their utilisation of the urease enzyme, and cyanobacteria respond to Ni independently of the nitrogen source, illustrating the importance of the NiFe hydrogenase and Ni-SOD enzymes (Price and Morel, 1991; Dupont et al., 2008a, 2008b, 2010; Egleston and Morel, 2008; Ho, 2013). These studies clearly demonstrate the essential bioactive role of Ni and emphasize the link between the biogeochemical cycles of Ni and nitrogen (N).

Despite these important bioactive roles, and unlike other bioactive trace metals, Ni concentrations in the surface ocean are never depleted to very low concentrations, instead reaching a ubiquitous minimum of around 1.7 nmol/L (GEOTRACES Intermediate Data Product Group, 2021). For this reason, Ni has not generally been considered as a limiting trace metal in the ocean, and consequently remains under-studied compared to other bioactive elements. Interestingly however, a strong contrast in Ni vertical distributions between high and low-latitude oceanic regions has been reported, with surface depletion only measured at low latitudes (Bruland, 1980; Middag et al., 2020; Sclater et al., 1976). Similarly, a difference between high and low latitudes is observed for Ni isotopes, with a significant fractionation in Ni isotopes in the surface only observed at low-latitude stations (Archer et al., 2020; Bian et al., 2024; Cameron and Vance, 2014; Lemaitre et al., 2022; Takano et al., 2017; Wang et al., 2019; Yang et al., 2021, 2020). This isotope fractionation demonstrates that one or more specific processes affect Ni biogeochemistry in low-latitude surface waters. Three hypotheses have been proposed so far to explain heavy Ni isotopes in the surface low latitude ocean. The first postulates the existence of a residual non-bioavailable Ni pool that is complexed to organic ligands, so that the very slow dissociation kinetics of these organic complexes (Mackey et al., 2002) would limit Ni uptake by phytoplankton species. This complexed non-bioavailable Ni reservoir is expected to be isotopically heavy (Archer et al., 2020). A second hypothesis suggests that surface Ni could correspond to a residual pool, fractionated to heavy isotope compositions by biological uptake of light isotopes, following exhaustion of macronutrients in low-latitude regions (John et al., 2022, 2024). A third view postulates that the biogeochemical divide between low and high latitudes could be due to specific enzymatic needs between different ecosystems (Lemaitre et al., 2022).

https://doi.org/10.5194/egusphere-2025-6336
Preprint. Discussion started: 19 January 2026

It is this latter proposition that is our main target for investigation here. In this view, the role of Ni could be especially important in low-latitude regions where dissolved inorganic nitrogen is often limiting, leading to greater urease activity and creating a niche for diazotrophs. High light conditions are also common in low-latitude surface waters, increasing the concentration of superoxide species and thus leading to greater utilisation of the Ni-SOD enzyme. The Ni-SOD enzyme plays another important role for diazotrophs as it has been shown to protect the nitrogen fixation process. Specifically, the 'nitrogenase' enzyme, responsible for the nitrogen fixation process (*nifH* gene), is vulnerable when exposed to reactive oxygen species (Chen et al., 2022). The NiFe hydrogenase enzyme also acts as a protector for the nitrogen fixation process and produces energy, which in turn is used for nitrogen fixation (Li et al., 2022). Because of these different enzymatic roles in nitrogen metabolism, disentangling the specific process (or processes) leading to low-latitude surface water Ni depletion and isotope fractionation is challenging.

Our understanding of the role of microbial communities and their activity in driving biogeochemical cycles has been revolutionised by the rise of omic technologies, which has led to significant advances in the description of taxonomic and functional diversity of microorganisms from a variety of complex ecosystems, including the ocean (White et al. 2016). Metagenomics, *i.e.* the sequencing of DNA from environmentally sampled microbial communities, has changed our understanding of planktonic taxonomic and functional diversity (Sunagawa et al., 2015; de Vargas et al., 2015). Sequenced metagenomics samples, called metagenomes, are composed of short DNA fragments from whole planktonic populations. The assembly of these short fragments called reads into longer sequences called contigs allows to recover a large fraction of the genes present in a specific environment. By computing the relative number of reads matching the DNA sequence composition of the different contigs in each sample, it is then possible to quantify the relative abundance of each contig and each gene in the original sampled population. In addition, sequence comparison with functional databases gives access to the potential metabolic role of the detected genes, helping to decipher the genetic potential of natural populations present in the environment (*e.g.,* Vernette et al. 2022). Genes can also be taxonomically annotated by comparing their contig of origin with reference databases of genome taxonomy. Metagenomics data are thus ideal for investigating the impact of bio-mediated processes on nutrient distributions in the ocean (Levine and Leles, 2021). For example, such an approach has been used to identify urease as a key enzyme for adaptation to nitrogen-limited environments in the widespread *Thaumarchaeota* (Alonso-Sáez et al., 2012). The approach has also been used to show that Ni-binding SOD is prevalent in *Synechococcus* strains thriving in Fe-replete waters (Doré et al., 2023), while it is present in all known strains of *Prochlorococcus* and widespread in heterotrophic bacteria and archaea (Sutherland et al., 2021). Metagenomic surveys of hydrogenase diversity across terrestrial and aquatic ecosystems have highlighted hydrogen metabolism as an underestimated energy source for microbial growth (Greening et al., 2016). Comparative genomics and metagenomics have thus highlighted the role of Ni-related enzymes across a variety of organisms and ecosystems. However, to our knowledge, no study has investigated all known Ni-related enzymes through large scale metagenomics in the marine environment.

Here, for the first time, we couple metagenomics to data for Ni concentrations and δ^{60}Ni measured in samples collected from the upper 1000 m of the Atlantic sector of the Southern Ocean, and along a transect between Tasmania and Antarctica as part

https://doi.org/10.5194/egusphere-2025-6336
Preprint. Discussion started: 19 January 2026

of the Antarctic Circumnavigation Expedition (ACE). The data complement the limited Ni isotope database in the ocean, and the high-resolution of the shallow depth profiles enables us to advance our understanding of surface processes driving Ni cycling. This study also explores the suggestion that specific microbial communities and their enzymatic needs may play a role in the oceanic Ni biogeochemical divide.

2 Material and methods

2.1 Study area

During the ACE cruise (December 2016-March 2017, R/V Akademik Tryoshnikov), seawater samples for Ni isotopes were collected at 10-12 depths in the upper 1000 m at 8 stations from Leg 2 (stations 8-11) and Leg 3 (stations 22-25), in the Atlantic and Pacific sectors of the Southern Ocean respectively (Figure 1). These stations span the major Antarctic Circumpolar Current (ACC) fronts around Antarctica (Orsi et al., 1995): the Sub-Tropical Front (STF), the Sub-Antarctic Front (SAF), the Polar Front (PF), the Southern ACC Front (SACCF) and the Southern Boundary of the ACC (SB). These fronts divide the Southern Ocean into several broadly uniform physical and biogeochemical zones. Macronutrient abundances and phytoplankton communities differ in the surface waters of these frontal zones. Upwelled nutrient-rich waters reach the surface south of the PF, with nutrient concentrations decreasing due to phytoplankton uptake during transport northwards. Intense diatom blooms occur around the PF, depleting silicate in surface waters north of the PF, whereas phosphate and nitrate decrease more gradually until depletion at the SAF (Sarmiento et al., 2004). As a result, meridional changes also occur in phytoplankton communities: diatoms requiring Si for growth are the dominant species as far north as the PF and continue to contribute to the surface communities near the SAF; calcifiers such as coccolithophores play an important role between the SAF and the STF; pico-phytoplankton such as cyanobacteria tend to dominate the phytoplankton community north of the STF (Antoine et al., 2020). Chlorophyll-*a* (chl-*a*) concentrations, an indicator of phytoplankton biomass, were generally low along the ACE track (< 0.5 mg/m^3; Robinson et al., 2021), which is typical of the high nutrient-low chlorophyll (HNLC) Southern Ocean. However, high chl-*a* were observed in surface waters near shelves, subantarctic islands or in polynya systems near Antarctica (chl-*a* concentrations = 1.9 mg/m^3 at station 11, within the Mertz glacier polynya).

2.2 Sample collection and analytical methods for Ni concentrations and isotopes

2.2.1 Seawater sampling

Samples were collected using a trace metal clean rosette equipped with acid-cleaned, Teflon-coated, 10 L X-Niskin bottles, following the recommendations of the GEOTRACES cookbook (Cutter et al., 2017). The rosette was attached to a Dynema line with a dedicated, custom-designed winch, allowing the rosette to be deployed from and landed on the main deck directly outside the trace metal clean container. Immediately after recovery, all the Niskin bottles were covered at each end with plastic bags to minimise contamination and were then transferred into the clean container (Class-100) for sampling. Filtered seawater

https://doi.org/10.5194/egusphere-2025-6336
Preprint. Discussion started: 19 January 2026

samples for dissolved trace metals were collected by gravity filtration using acid-cleaned 0.2 µm AcroPak cartridge filters (Pall). Between 1 and 4 L of filtrate were collected in acid-cleaned low-density polyethylene (LDPE) bottles and stored at room temperature. Back at the home laboratories at ETH Zurich, the filtered seawater samples were acidified to pH ~ 2 by addition of concentrated hydrochloric acid (HCl; Merck AnalaR grade, further purified by double sub-boiling distillation) and left for at least 3 months before processing. The samples described here have previously been analysed for dissolved Cd, Zn and Fe concentrations and isotopes (Sieber et al., 2019, 2020, 2021).

2.2.2 Dissolved Ni concentration and isotope analyses

All samples were processed at ETH Zurich under clean laboratory conditions (Class 1000) within clean laminar flow hoods (Class 10), using only trace metal clean Savillex PFA labware. All water used was ultrapure (≥18.2 MΩ.cm) and all acids and reagents were Merck AnalaR grade, further purified by double sub-boiling distillation.

The methods used here have been previously described and published by the ETH group (Archer et al., 2020; Lemaitre et al., 2022; Wang et al., 2019). Prior to ion exchange purification, a ^{61}Ni-^{62}Ni double-spike was added to reach a sample-to-spike ratio of 1:1 and the samples left to equilibrate for 48 hours. Samples were then adjusted to pH 5.0 ± 0.3 using an ammonium acetate buffer, before loading onto a preconcentration column containing an ethylenediaminetriacetic acid chelating resin, sold commercially as Nobias PA1 (Hitachi High Technologies; Sohrin et al., 2008). The seawater matrix was eluted using 30 mmol/L ammonium acetate buffer and the metals were extracted from the resin using 1 mol/L nitric acid. Trace metals were then separated from each other through an anion exchange column (Bio-Rad AG MP-1M resin). The Ni fraction was further purified using a miniaturised version of the Nobias preconcentration column and a small anion column (to remove any residual matrix cations, Zn or Fe).

Isotope analyses were performed on a Thermo Neptune Plus Multi-Collector-ICPMS operated in low resolution mode at ETH Zurich. Samples were introduced into the mass spectrometer in 0.3 mol/L nitric acid via a CPI PFA nebuliser (50 µL/min) attached to a Cetac Aridus II desolvating nebuliser system, using standard Ni sample and H-skimmer cones. In addition to the Ni isotopes, ^{56}Fe and ^{57}Fe were measured to monitor and correct for potential interference from ^{58}Fe on ^{58}Ni. Mass discrimination was corrected using the double spike, as detailed previously (Cameron and Vance, 2014). Ni stable isotope ratios are all expressed in standard delta notation relative to the primary NIST SRM 986 Ni standard, as follows:

$$\delta^{60}\mathrm{Ni}\ (‰) = \left[\frac{(^{60}\mathrm{Ni}/^{58}\mathrm{Ni})_{\mathrm{sample}}}{(^{60}\mathrm{Ni}/^{58}\mathrm{Ni})_{\mathrm{NIST\ SRM\ 986}}} - 1\right] \times 1000$$

Repeat measurements of secondary standards Nod-A1 and Nod-P1 (USGS Fe-Mn nodules digested and passed through the Ni column chemistry) were used to evaluate the long-term reproducibility of the isotope analyses. Over the course of this and parallel studies, we obtained δ^{60}Ni = 1.04 ± 0.07 ‰ (2SD, n=446) for NOD-A1 and δ^{60}Ni = 0.34 ± 0.07 ‰ (2SD, n=590) for NOD-P1. These values are consistent with previously reported values (Gueguen and Rouxel, 2021). Internal errors of the

https://doi.org/10.5194/egusphere-2025-6336
Preprint. Discussion started: 19 January 2026

instrumental analyses, propagated through the double spike algebra, are given in Table S1. The uncertainties on Ni isotope compositions shown in Figure 2 are either the internal or the long-term error, whichever is larger. Concentrations reported herein were calculated from the double-spike data using the isotope dilution approach.

This laboratory has demonstrated agreement for Ni concentrations and isotopes with the GEOTRACES IDP (GEOTRACES Intermediate Data Product Group, 2021). The ACE Ni concentrations and isotope compositions have been approved by the GEOTRACES Standards and Intercalibration (S&I) committee and have been released in the GEOTRACES IDP2025. Furthermore, the ACE Ni data from the Atlantic sector were compared to those of Archer et al. (2020) and Cameron and Vance (2014) and showed good agreement in the context of variability in other parameters such as phosphate concentrations and temperatures (Figure S1).

2.3 Analytical methods and clustering techniques for metagenomics

2.3.1 Metagenomics sampling and sequencing protocols

A total of 218 metagenomic samples were collected at 34 different stations over the ACE cruise (Faure et al., 2025). In this study, we focus only on the 48 samples taken at trace-metal stations, where Ni-related measurements are also available. Water was sampled from Niskin bottles during rosette upcast and filtered into different size fractions: 0.2 - 3 µm, 0.2 - 40 µm and 3 - 200 µm. Given the small number of 0.2 - 40 µm samples (6 in this study) and their high genomic similarity with 0.2 - 3 µm samples (as estimated by SIMKA using all ACE metagenomes; Benoit et al. 2016, Faure et al. 2025), the 0.2 - 3 µm and 0.2 - 40 µm samples were combined into a small size fraction and treated separately from the large (3 - 200 µm) size fraction (Faure et al., 2025). DNA extraction and library preparation was achieved using *Tara Oceans* protocols. Briefly, after filter cryogrinding, DNA was extracted using total RNA/DNA Purification and Nucleospin RNA/DNA Buffer Set (MACHEREY-NAGEL). Metagenomic libraries were prepared using the Illumina kit according to manufacturer instructions. DNA libraries were sequenced on a Novaseq 4000 instrument, with a target of 100M paired-end reads per library (2x 150bp; 500bp insert size). The mean number of sequenced paired-end reads across the 218 ACE samples ended up at 138.5M (142M across the 48 samples considered in this study), exceeding the target of 100M in all but 7 samples.

2.3.2 Selection of gene clusters related to nickel

Different bioinformatic tools are used here for annotating genes with a function (eggNOG which includes PFAM, and KEGG), for annotating contigs with a taxonomy (MMSeqs taxonomy and Kraken) and for clustering genes (CD-Hit and AGNOSTOS clusters). The schematic presented in Figure S2 summarises the different methods applied to the metagenomic data in this study.

Briefly, short-reads were quality-filtered and assembled by samples using illumina-utils v2.3 (Eren et al. 2013, Minoche approach with default parameters) and MegaHit v1.2.9 (Li et al. 2015, minimum contig length of 1000, meta-sensitive mode). An average of 94.9% of read pairs passed the filtering step across all ACE samples (94.8% considering only the 48 samples

https://doi.org/10.5194/egusphere-2025-6336
Preprint. Discussion started: 19 January 2026

from trace-metal stations). Tables summarizing quality-filtering and assembly steps statistics are available from the doi: 10.6084/m9.figshare.29127848. Open-reading frames (ORFs, *i.e.,* fragment of DNA spanning from a start codon to a stop codon) were detected in all the 68,074,004 obtained contigs using Prodigal v2.6.3 (Hyatt et al., 2010), and clustered using the AGNOSTOS pipeline (Vanni et al., 2022) with default parameters to produce 30,123,228 AGNOSTOS gene clusters (AGC), of which 765,003 were discarded as low quality. In parallel, non-dereplicated ORFs were clustered at 95% similarity and 90% coverage using CD-Hit (Li and Godzik, 2006), creating 89,739,060 unigenes that were functionally annotated using the eggNOG mapper v2.1.0 using default parameters (Huerta-Cepas et al., 2017) and KOFamScan v1.3.0 (Aramaki et al., 2020) set with an e-val threshold of 0.01. Both eggNOG and KEGG databases allow a comprehensive characterization and analysis of the gene families, providing functional annotations at different levels of precision. Unigenes of interest for Ni were selected according to their functional annotation:

- Unigenes with eggNOG annotations containing one of the words "urease", "NiFe" or the combination of "superoxide" and "dismutase" (in any of eggNOG-mapper output columns, including narrow orthologous group (OG) description, best OG description and PFAM).
- Unigenes annotated to a KEGG ID corresponding to urease, NiFe hydrogenase or superoxide dismutase (K01427, K01428, K01429, K01430, K03187, K03188, K03189, K03190, K03192, K14048, K00437, K05586, K05587, K05588, K18005, K18006, K18008, K00518, K04564, K04565, K04569, K16627).

All AGC containing at least one non-dereplicated gene belonging to a unigene cluster of interest for Ni were considered of interest for Ni as well. When used, AGC-level eggNOG, PFAM and KEGG annotations are defined as the modal value from the annotations of all cluster's members.

All contigs containing at least one ORF clustering in a unigene annotated to a Ni-related enzyme were taxonomically annotated using MMSeqs2 v14.7e284 with the UniREF90 reference database (Suzek et al., 2015), and Kraken2 (Lu et al., 2022) with the GTDB database (Parks et al., 2022). AGC-level taxonomic annotations were defined as the most frequent in each cluster. Yet, considering the potentially higher taxonomic diversity than functional diversity within cluster, individual ORF annotations were investigated for all clusters of interest (Tables 1, S2).

In addition to Urease, NiFe hydrogenase, and superoxude dismutase, we investigated the potential presence of nitrogen fixation enzymes in our samples but could not show any evidence, suggesting that potential diazotrophs are not present (see Supplementary Information for more details on the methods and results).

It should also be noted that our bioinformatic method does not allow the analysis of the presence of eukaryotes in as much detail as bacteria and archaea. Indeed, genes from eukaryotic organisms may comprise coding (exons) and non-coding (introns) DNA sequences, which makes their detection in metagenomic assemblies more difficult than for bacteria and archaea (Stanke et al., 2004). Although there is a significant amount of eukaryotic contigs and genes in the large size fraction (Faure et al., 2025), our conclusions on the role of eukaryotes in driving Ni isotope fractionation in surface waters of our ACE stations will have to be complemented by genome-resolved and (meta-)transcriptomics studies. Another limitation of our study comes from

https://doi.org/10.5194/egusphere-2025-6336
Preprint. Discussion started: 19 January 2026

the significant fraction of uncharacterised sequences due to an absence of match in current reference databases, estimated to represent 38% of the ACE reference gene catalog (Faure et al., 2025). The ACE cruise is the first large-scale metagenomic sampling of the Southern Ocean, and considering the uniqueness of its ecosystem, it is not surprising that a high percentage of unmatched sequences is observed.

2.3.3 Computation and normalisation of function- and cluster-level coverage

Normalised coverages from unigenes and AGNOSTOS gene clusters (AGC) were retrieved from the abundance matrices computed in Faure et al. (2025). Briefly, quality-filtered short reads were mapped onto the ACE contig database (*i.e.*, corresponding to all contigs assembled via ACE metagenomes) to produce contigs-level coverage and detection (% of the contigs covered at least at 1X) profiles, using Bowtie v.2.4.5 (Langmead and Salzberg, 2012). Anvi'o v7.1 (Eren et al., 2015) was used to extract ORF coverage from their parent contigs. Coverages for all members of each unigene and AGNOSTOS cluster were summed to obtain unigene- and cluster-level coverages. A threshold of detection was applied at unigene and cluster level to avoid false-positive coverage values due to mapping mistakes and read dilution across conserved domains. Detection at cluster level was defined as $\text{DetectionCluster} = \max(\text{Detection}_{\text{Cluster members}})$ for both unigenes and AGNOSTOS clusters. Based on collector curves computed at various levels of detection thresholds, the maximum was set at 60%, *i.e.,* all coverage values for which no ORF had a value of at least 60% detection were turned to 0 (Faure et al., 2025). All remaining coverage values were rounded to the nearest integer before normalisation using the relative log expression method from the DeSeq2 R package (Love et al., 2014), which estimates size factors to correct for library size and composition biases. To further limit the impact of compositionality and total sample coverage biases, which can impact observed correlations when summing up abundances of large amounts of unigenes (*e.g.* grouping unigenes by broad functional annotations), we used robust Centered-Log Ratio (r-CLR) and relative transformed abundances computed on all ACE unigenes/AGNOSTOS gene clusters. Considering the similarity in the results obtained with the two transformations, we present results based on the easier to interpret relative abundances in Figures 3 and S3, while equivalent graphs computed on r-CLR transformed data are available in Figure S4.

Different functional annotation levels were investigated: 1) by summing relative unigene abundances into broad functional groups: urease, NiFe hydrogenase or superoxide dismutase (Figure S3); 2) by summing relative unigene abundance for each unique KEGG functional annotation; 3) by summing relative unigene abundance for each unique eggNOG functional annotation (using best OG description, Figure 3); 4) by summing relative unigene abundance for each unique PFAM functional annotation (Figure 3). Since log-ratio transformations are not additive, we computed the mean of transformed abundances instead of sums when working on r-CLR transformed data (Figure S4).

https://doi.org/10.5194/egusphere-2025-6336
Preprint. Discussion started: 19 January 2026

2.3.4 Investigating the correlation between cluster coverage and isotope fractionation

All statistical investigations of unigenes/AGC/broad functional groups abundance in relation to Ni measurements were conducted separately on the small and large size fractions. In matrices corresponding to each size fraction, clusters absent in all samples were removed.

Correlations between the various metagenomic coverage values and Ni isotope fractionation were computed using the rank-based Spearman coefficient and tested using a two-sided permutation-based approach (PermCor R package, 1000 permutations). Obtained p-values were adjusted using the Bonferroni-Hochberg correction.

Redundancy analyses (RDA) were achieved on r-CLR-transformed AGNOSTOS gene cluster abundances using the R package vegan v2.6-2 (Oksanen et al., 2022). Only clusters with more than one positive r-CLR-transformed abundance were considered, *i.e.* 719 AGNOSTOS gene clusters in the small size fraction and 232 AGNOSTOS gene clusters in the large size fraction. The significance of each RDA was tested using the permutations-based test implemented in the anova.cca function. All scripts necessary to reproduce the statistical analysis achieved in this paper are available at: https://github.com/EmileFaure/Nickel_Omics.

3 Results

3.1 Latitudinal differences in Ni concentrations and isotopes

Dissolved Ni concentrations and isotope compositions for all ACE stations are presented in Figure 2, and together with macronutrient concentrations and other parameters in Table S1. Overall, dissolved Ni concentrations range from 2.97 to 8.29 nmol/L and exhibit typical 'nutrient-like' profiles, with lower concentrations in surface waters compared to deep. However, there is a strong contrast between the profiles depending on latitude. Only subtle variations are observed with depth at high-latitude stations, south of the Sub-Antarctic Front (stations 9, 10, 22, 23, 24) with only a 1% median concentration increase between the surface and 100 m. Station 11, near the Mertz Glacier, is an exception among high-latitude stations as it is characterised by a strong decrease of Ni concentrations in the upper 50 m. This pattern is more similer to stations located north of the Sub-Antarctic Front (stations 8 and 25). At these three stations (stations 8, 11, 25), the median concentration increase from the surface to 100 m is 21 %. Stations 8 and 25, north of the Sub-Antarctic Front, have lower surface Ni concentrations (between 3 and 4 nmol/L) compared to other stations (between 5 and 7 nmol/L). Depth profiles of nitrate and phosphate concentrations follow similar trends, with lower concentrations in the surface compared to the deep ocean, and with lower surface concentrations at stations north of the Sub-Antarctic Front and at the Mertz Glacier (stations 8, 25 and 11; ~10 µmol/L nitrate and ~0.5 µmol/L phosphate in the upper 50 m) compared to other stations (~20 µmol/L nitrate and ~1.5 µmol/L phosphate in the upper 50 m).

The overall observed variability in Ni isotope composition is 0.6 ‰, ranging from 1.09 to 1.68 ‰ for all ACE stations. As for Ni concentrations, variations in δ^{60}Ni are small for high-latitude stations, usually within the range of the average deep ocean

https://doi.org/10.5194/egusphere-2025-6336
Preprint. Discussion started: 19 January 2026

value (1.34 ± 0.12 ‰ at depth > 500 m, mean ± 2SD, shaded band in Figure 2; Cameron and Vance, 2014; Takano et al., 2017; Wang et al., 2019; Archer et al., 2020; Yang et al., 2020, 2021; Lemaitre et al., 2022; Bian et al., 2024; this study). Conversely, the Mertz Glacier (station 11) and stations north of the Sub-Antarctic Front (stations 8 and 25) exhibit different depth profiles: as Ni concentrations decrease towards the surface, the isotope composition becomes heavier, with δ^{60}Ni reaching 1.68, 1.63, 1.65 ‰ respectively. Such high δ^{60}Ni values have also been observed in surface low-latitude stations in the Atlantic and Pacific oceans (Archer et al., 2020; Bian et al., 2024; Lemaitre et al., 2022; Takano et al., 2017; Yang et al., 2021, 2020). The data reported here thus extend the latitude range of this surface fractionated Ni, in addition to identifying the same signature in a coastal and in a polynya environment.

3.2 Relationship between Ni distributions and metagenomics

The relationships between metagenomics and δ^{60}Ni were studied at various biological precisions, as described below and in Figure S2: 1) by summing unigenes into broad functional groups, and 2) by investigating AGC, *i.e.*, refined gene clusters that go beyond broad functional annotations.

3.2.1 Urease and superoxide dismutase enzymes associated with Ni fractionation

In the first approach, we investigated correlations between δ^{60}Ni and relative abundances of unigenes identified as related to the three selected enzymes involving Ni, comprising 91 unique eggNOG descriptions, 77 PFAM annotations and 14 unique KEGG functional annotations (not accounting for double KEGG functional annotations such as K03188, K03190 when both IDs are present independently). Sorting abundances into SOD, urease or NiFe hydrogenase functional groups did not lead to significant correlations with δ^{60}Ni, but positive correlations could be observed for SOD in the small size fraction and urease in the large size fraction (Figure S3). Regarding eggNOG best description annotation-level abundances, two of the Spearman correlation tests with δ^{60}Ni were significant (Figure 3). The COG2370 hydrogenase urease accessory protein annotation was significantly correlated to δ^{60}Ni in the small size fraction (adj. p-value = 0.04), while the UreD urease accessory protein was significantly correlated to δ^{60}Ni in the large size fraction (adj. p-value = 0.03). The COG2370 annotation corresponds to a conserved domain typically involved in the maturation and activation of metalloenzymes requiring Ni as a cofactor, including both NiFe hydrogenase and urease. Removing Mertz samples from correlation tests, we found 3 additional annotations to be significantly correlated to δ^{60}Ni in the small size fraction (COG2370 correlation remaining significant, adj. p-value = 0.03), superoxide dismutase (adj. p-value < 10^{-3}), uracil-DNA glycosylase (adj. p-value < 10^{-3}) and superoxide dismutase copper chaperone activity (adj. p-value = 0.04, likely unrelated or indirectly related to Ni fractionation considering its copper-related annotation). Uracil-DNA glycosylase has a role in DNA repair and is not directly linked with nickel. However, the 451 unigenes annotated to Uracil-DNA glycosylase as best OG description in our selection all showed "UreE urease accessory protein, C-terminal domain" as narrow OG description. UreE directly helps nickel incorporation into urease and shares domain and structure similarities with Uracil-DNA glycosylase: the SMART domain SM00987 (C-terminal domain of UreE) belongs to the structural and functional superfamily of Uracil-DNA glycosylase-like superfamily (SSF52141) and often maps on the

https://doi.org/10.5194/egusphere-2025-6336
Preprint. Discussion started: 19 January 2026

same proteins as SM00986 (Uracil-DNA glycosylase). These similarities may explain the potential confusion in the functional annotation. In the large size fraction, there are no significant correlations remaining after removing the Mertz samples, and the observed significant correlations do not hold when considering r-CLR transformed data, despite a similar jump in abundance in Mertz samples (Figure S4). Correlations between PFAM annotations and δ^{60}Ni were not significant when accounting for all samples. Removing Mertz samples led to two significant correlations in the small size fraction: Sod_Ni (Ni-containing superoxide dismutase; adj. p-value < 10^{-3}) and LysE,UDG (Lysine exporter and/or uracil-DNA glycosylase; adj. p-value = 0.03, corresponding to unigenes with Uracil-DNA Glycosylase as best OG description, potentially related to UreE as aforementioned). Although insignificant (p-value = 0.005, adj. p-value = 0.1), the relationship between the UreD,UreF PFAM annotation (activation of urease) and δ^{60}Ni illustrates the positive anomaly in urease abundances at Mertz in the large size fraction. None of the Spearman correlation tests between δ^{60}Ni and KEGG functional annotation-level abundances produced an adjusted p-value below 0.05, thus we do not discuss KEGG KOs below.

3.2.2 Different gene clusters associated with δ^{60}Ni across stations

In the second approach, we investigated the relationship between δ^{60}Ni and individual AGC (*i.e.*, ORFs with similar amino acid sequences), allowing the division of broad functional categories into smaller, more functionally and evolutionarily refined, groups. A total of 1966 AGC were identified as containing at least one ORF annotated as one of the three selected enzymes involving Ni. The RDA were significant for each size fraction (p-values < 10^{-3}), suggesting a significant link between AGC abundances and Ni distributions. The adjusted R-squared of the RDA was 16.9 % for the small size fraction and 28.7 % for the large size fraction. In the small size fraction, RDA1 explained 13.6 % of the variance and was correlated with δ^{60}Ni, *i.e.* samples with high values of δ^{60}Ni correspond to the positive side of the x-axis (Figure 4a). RDA2, accounting for 9.1 % of the variance, was correlated to Ni concentrations and anti-correlated to δ^{60}Ni. The three AGNOSTOS gene clusters (AGC) located above 0.5 on axis 1 and below -0.5 on axis 2 were extracted as particularly correlated to δ^{60}Ni. Station 11 (Mertz) was mostly correlated to axis 1, while stations 8 and 25 (north of Sub-Antarctic Front) were mostly correlated to axis 2. From these observations, all 13 AGC located above 0.5 on axis 1 and between 0 and -0.5 on axis 2 were extracted as particularly correlated to station 11. Similarly, 24 AGC were extracted as particularly linked to stations 8 and 25 (axis 2 < -0.5 and 0 < axis 1 < 0.5, or axis 2 < 0.75 and axis 1 < 0). In the large size fraction, RDA1 explained 28.9 % of the variance and was mostly correlated to Ni concentrations, while RDA2 explained 8.2 % and was anti-correlated with δ^{60}Ni (Figure 4b). AGC_14687886, nearly orthogonal to axis 1 and well projected on the negative side of axis 2, was identified as particularly corelated to δ^{60}Ni (as in the small size fraction). Among other AGC located below -0.5 on axis 2, all those with positive positions on axis 1 were associated with station 11, while all those with negative positions were associated with stations 8 and 25. Table 1 describes functional and taxonomic annotations of selected AGC, while a complete description of all extracted clusters is available in Table S2.

https://doi.org/10.5194/egusphere-2025-6336
Preprint. Discussion started: 19 January 2026

4 Discussion

4.1 Ni concentration and isotope cycling in the Southern Ocean

Overall, the new ACE dataset follows established oceanic Ni-δ^{60}Ni systematics and is consistent with the biogeochemical divide typically reported between low and high latitudes. The data further refine this divide by demonstrating that Ni fractionation occurs between the Sub-Antarctic and Sub-Tropical Fronts. However, located next to the Mertz glacier, ACE station 11 represents an exception. A decrease in Ni concentrations is accompanied by an increase in δ^{60}Ni in the upper 50 m (Figure 2), which leads to Ni and δ^{60}Ni systematics at this station that are significantly above the trend described by other high-latitude data (Figure 5).

At station 11, located within an Antarctic polynya, surface concentrations of macronutrients and other trace metals are also lower than in the surface waters of other high-latitude stations (Janssen et al., 2020; Sieber et al., 2019, 2020, 2021). The lower salinity suggests a meltwater input, but the above authors demonstrated that the resultant dilution of surface seawater cannot explain the lower nutrient concentrations. Instead, they suggest that lower macro- and micronutrient concentrations are due to substantial phytoplankton uptake at station 11, consistent with the high chl-*a* concentrations observed during the cruise (Figure 1). Sieber et al. (2021) showed that Fe concentrations and isotopes at the Mertz station could be described with a closed-system Rayleigh-type fractionation with an alpha (α) value of 0.999, suggesting that a single process dominates the isotope fractionation. The authors attributed the removal of isotopically light Fe to phytoplankton uptake (Sieber et al., 2021), in line with a significant Fe uptake rate at the same station (Fourquez et al., 2023). Likewise, the clear evolution towards heavy Ni isotope compositions in the upper 100 m of station 11 follows a closed-system Rayleigh fractionation, with $\alpha = 0.99925$ (Figure 6). Such fractionation cannot be explained by physical mixing. Indeed, surface waters at station 11 consist of upwelled Circumpolar Deep Water (σ_Θ CDW ~ 27.6 – 27.8 kg/m^3), whose Ni isotope composition is typical of the average deep world ocean (δ^{60}Ni = 1.31 ‰). This contrasts with the surface of station 11 (δ^{60}Ni > 1.60 ‰), indicating that the isotope fractionation near the surface of station 11 must instead be explained by a local process. To determine whether the isotope fractionation results from biological uptake, phosphate depletion in the water column is compared to Ni depletion in the same samples. At station 11, phosphate and Ni are respectively depleted by 56 and 31% between 80 m and the surface. The depletion of both elements is more pronounced than observed at station 10, where phosphate and Ni are only depleted by 4 and 1%, respectively. This indicates an enhancement of biological utilisation at station 11 relative to the adjacent station. These observations are further supported by metagenomics investigations of biological diversity within the Mertz polynya compared to the rest of ACE samples (Faure et al., 2025). Indeed, Mertz samples were very different from all other Sub-Antarctic Surface Water samples, displaying exceptional genomic compositions explained by the abundance of diatoms and a variety of associated heterotrophic bacteria specialized in the use and recycling of organic matter (Faure et al., 2025).

The fractionation factors at stations 8 and 25, north of the Sub-Antarctic Front, are 0.9988 and 0.99905 respectively, indicating a removal of light Ni isotopes in surface waters, likely due to biological uptake. These fractionation factors are the highest ever reported (Takano et al., 2017; Archer et al., 2020; Yang et al., 2021; Bian et al., 2024), suggesting that different microbial

https://doi.org/10.5194/egusphere-2025-6336
Preprint. Discussion started: 19 January 2026

communities and requirements (e.g., due to Fe limitation) may influence the isotope effect. It is also possible that the systematics between Ni and δ^{60}Ni observed at these two stations may not reflect local processes and could alternatively be due to advection of signatures set elsewhere, as suggested to explain the chromium (Cr) distribution in the ACE samples (Rickli et al., 2019). The shallow samples (σ_Θ < 26.6 kg/m^3) as well as underlying samples (26.7 < σ_Θ < 27.1 kg/m^3) associated with Sub-Antarctic Mode Water originating from the Southern Ocean (σ_Θ SAMW ~ 26.8 kg/m^3) are characterised by strong linear relationships between salinity and Ni concentration (R^2 > 0.82; Figures 7a and 7b), consistent with Rickli et al. (2019). However, unlike for Cr isotopes, the relationships between salinity and δ^{60}Ni for both density intervals are weak (R^2 < 0.17; Figures 7c and 7d). This suggests that Ni isotope distributions at stations 8 and 25 may not be consistent with conservative mixing. Similarly to station 11, biological uptake may thus be a local process leading to higher δ^{60}Ni values in the surface waters of these northerly stations.

4.2 Metabolic potential in waters where Ni fractionates

Nickel isotope fractionation in nutrient-depleted low-latitude waters was found to correlate with nitrogen fixation in the North Atlantic (Lemaitre et al., 2022). The absence of nitrogen-fixing potential in microbial communities observed across ACE samples suggests that nitrogen fixation cannot explain the Ni isotope fractionation seen in this study (see Supplementary Information for more details on the method and results). This coincides with the relatively high nitrate levels and the low abundances of cyanobacteria across the whole transect (Antoine et al., 2020; Faure et al., 2025). Other processes are therefore required to explain the Ni distributions observed in our samples.

Focusing first at a broad functional scale (*i.e.* enzyme level or KEGG, eggNOG and PFAM functional annotation levels, see section 2.3.3 and 3.2.1), the links between Ni isotopes and the abundances of the SOD, urease and NiFe hydrogenase enzymes are investigated. No correlation between Ni isotopes and the abundance of the NiFe hydrogenase enzyme is found, independently of the size fraction and functional annotation level (Figure S3). In contrast, positive correlations between SOD and δ^{60}Ni are observed in the small size fraction, maintained across different functional annotation levels, but are only significant when Mertz samples are excluded (section 3.2.1, Figures 3a, S4). Similarly, the abundance of two enzymes potentially involved in Ni incorporation in urease co-vary with δ^{60}Ni when Mertz samples are excluded: UreE, which is barely distinguished from Uracil-DNA Glycosylase in our annotations, and COG2370, which could also correspond to NiFe hydrogenase. Note that the presence of the NiFe hydrogenase is unlikely, given the absence of statistical signal between NiFe hydrogenase abundance and δ^{60}Ni in all other results. Our results in the small size fraction suggest therefore that prokaryotic SOD and urease enzymes may be involved in Ni consumption and fractionation, yet their low relative abundance in Mertz samples seem to indicate that Ni fractionation at station 11 is driven by other kinds of biological activity. In the large size fraction, the co-variation between the abundance of the urease enzyme and δ^{60}Ni is driven by station 11, where the relative abundances of some sub-units of urease increase by an order of magnitude compared to other stations (Figure 3b). This co-variation at station 11 appears especially strong for the UreD sub-unit, an accessory protein facilitating urease maturation after

https://doi.org/10.5194/egusphere-2025-6336
Preprint. Discussion started: 19 January 2026

incorporation of Ni^{2+} inside the cell. Our results for the large size fraction thus suggest that the Ni isotope fractionation at Mertz might be linked to Ni uptake by large or particulate-attached organisms for their utilisation of the urease enzyme.

In order to further investigate the protein repertoire specific to high-δ^{60}Ni sampling sites and the taxa carrying them, we switch our focus from broad function-based aggregations of unigenes towards refined gene clusters called AGC (see Figure S2, sections 2.3.4 and 3.2.2). We investigate the relationship between Ni concentrations and δ^{60}Ni (as environmental variables) and AGC that contained at least one gene related to Ni enzymes by running redundancy analyses (RDA, Figure 4). Several gene clusters emerge from these analyses as exhibiting strong correlations with δ^{60}Ni (in yellow in Figure 4), at stations 8 and 25 (in orange in Figure 4), and at station 11 (in red in Figure 4). This geographical difference may reflect the ecological partitioning observed between low- and high-latitude stations, with differences in taxonomic and functional compositions of microbial populations bearing enzymes using Ni (Tables 1 and S2). North of the Sub-Antarctic Front, in the small size fraction, 1 gene cluster annotated as NiFe hydrogenase, 5 as urease and 3 as Ni-SOD are strongly correlated for stations 8 and 25. The size of these Ni-SOD gene clusters (*i.e.*, the number of unique genes they contain) is relatively important, indicating that conserved forms of Ni-SOD genes are frequently found in the ACE metagenomic dataset, suggesting their widespread abundance in the Southern Ocean. In the large size fraction, stations 8 and 25 are correlated with 1 gene cluster annotated as Ni-SOD and 4 as urease, with the size of these latter being more important. The taxonomic annotations of these clusters indicate that the Ni-SOD is carried by diverse heterotrophic bacteria (*Opitutae*, *Planctomycetaceae*, *Piscirickettsiaceae*, *Alteromonadaceae*, *Porticoccaceae*) or by *Phaeocystis*, which is a common phytoplanktonic eukaryote across the Southern Ocean. On the other hand, urease is mostly carried by alphaproteobacterial families such as *Rhodobacteraceae* and *Roseobacteraceae*. In contrast, at station 11, the Ni-SOD enzyme (2 gene clusters) is carried by *Polaribacter* and *SAR92*, which are heterotrophic bacteria associated with the diatom bloom within the Mertz polynya at the sampling time (Faure et al., 2025), while urease (6 gene clusters) is carried by the blooming diatoms and associated *Rhodobacteraceae*. In addition, 3 gene clusters are directly linked to δ^{60}Ni, without being particularly associated with a station (Figure 4). These 3 gene clusters are all annotated as urease enzymes carried by proteobacterial families such as *Rhodobacteraceae* and *Roseobacteraceae,* highlighting the presence of these lineages at both high- and low-latitude stations.

4.3 Implications for global Ni isotope variability

The atypical Ni distribution at the high-latitude Mertz station (station 11) is likely due to its location in a very specific coastal and polynya environment. Indeed, this station was sampled during an intense diatom bloom (see chl-*a* concentrations in Figure 1) that led to the rapid proliferation of heterotrophic bacterial populations (highest total bacteria to chl-*a* ratio at station 11), acquiring substrates and energy from organic matter (Faure et al., 2025). In particular, diatom blooms have been shown to positively influence the growth of *Rhodobacteraceae* (Liu et al., 2019; Teeling et al., 2012), as supported by the annotation of many gene clusters associated with both groups in the Mertz samples (Tables 1 and S2). Moreover, urea has been shown to be an important N source for phytoplankton and prokaryotes near glaciers, where it can account for > 50% of the total dissolved N (Alonso-Sáez et al., 2012). It is therefore possible that diatoms and *Rhodobacteraceae* have used urea as a nitrogen source,

https://doi.org/10.5194/egusphere-2025-6336
Preprint. Discussion started: 19 January 2026

potentially impacting carbon and ammonium availability in a context of high primary productivity. This preferential uptake of urea at station 11 could have led to greater urease activity and Ni requirement.

At stations 8 and 25, north of Sub-Antarctic Front, the use of the urease enzyme by *Rhodobacteraceae* as well as by small phytoplankton species may also have contributed to the removal of isotopically light Ni. In addition, the Ni-SOD enzyme could also play a role in fractioning Ni isotopes at these lower latitudes. In our study, diverse heterotrophic bacteria carry the Ni-SOD enzyme, suggesting that no specific taxa may control the Ni biogeochemical divide between low and high latitudes. The global ocean Ni compilation suggests that Ni fractionation occurs in low latitudes, where cyanobacteria and diazotrophs dominate surface waters (Archer et al., 2020; Middag et al., 2020; Lemaitre et al., 2022). But in the present study area, at the edge of the low latitudes, cyanobacteria are scarce (less than 5% of the phytoplankton stock at stations 8 and 25) or absent at station 11 (Antoine et al., 2020), and nitrogen fixers are not detected. Similarly, the dominance of the urease and Ni-SOD enzymes over the NiFe hydrogenase enzyme in the ACE samples may be explained by the weaker role of this latter enzyme in regions where cyanobacteria and diazotrophs are minor communities.

5 Conclusion and perspectives

This study presents new Ni concentrations, Ni isotope compositions and metagenomics from different frontal zones of the Southern Ocean, using samples from the Antarctic Circumnavigation Expedition (ACE). We aim to explain the patterns observed for both Ni isotope fractionation and enzyme abundances in order to better understand the specific impact of biology on trace metal isotope distributions, information on which is very scarce in the literature. Surface samples at stations north of the Sub-Antarctic Front are characterised by elevated δ^{60}Ni (stations 8 and 25), confirming the Ni biogeochemical divide observed in the world ocean. Peculiar Ni distributions are however observed at the high-latitude station 11, near the Antarctic Mertz glacier: specifically low Ni concentrations associated with high δ^{60}Ni signals, matching low-latitude Ni trends. In line with preferential biological uptake, correlations between δ^{60}Ni and metagenomic abundances, as well as the significance of the RDA, suggest links between some enzymes, taxa and Ni isotope fractionation in the ACE samples. Some geographical differences are observed. The high relative abundance of the urease enzyme in samples from the Mertz Glacier suggests that diatoms and their associated *Rhodobacteraceae* alphaproteobacteria might rely on urea-based nitrogen, thereby consuming Ni and perhaps inducing Ni isotope fractionation. At low-latitude stations, both urease and Ni-SOD, carried by diverse heterotrophic bacteria and phytoplankton species from the small size fraction, are found to correlate with high δ^{60}Ni values. Therefore, our results suggest that the Ni biogeochemical divide likely reflects the combined activity of multiple microorganisms and enzymatic processes. While our data primarily reveal correlations between enzyme abundance and isotopic fractionation, the strength and significance of these relationships varied with functional databases and site selection. Understanding the potential biotic and abiotic drivers of the Ni biogeochemical divide will thus require further research beyond the first attempt made here. This should include a more complete analysis of organisms' metabolisms through genome-resolved approaches, especially to better integrate eukaryotes, combined with the use of metatranscriptomics to examine the activity of

https://doi.org/10.5194/egusphere-2025-6336
Preprint. Discussion started: 19 January 2026

nickel-related enzymes in addition to their presence. It is also necessary to go beyond correlations and quantify the impact of enzymatic activity on Ni drawdown and isotopic fractionation, through controlled lab experiments. Our study identifies different phytoplankton species and heterotrophic bacteria that may all play a role by utilising Ni, as already shown for Fe (Tortell et al., 1996), providing ideal candidate organisms and enzymes for future experiments.

Data availability

The new dissolved Ni isotope compositions (δ^{60}Ni) and concentrations, as well as the GEOVIDE macronutrient concentrations and CTD data are available in Table S1 and also publicly available through the GEOTRACES intermediate data product 2025 at BODC (https://www.bodc.ac.uk/geotraces/data/idp2025/). Raw metagenomics data are publicly available and can be downloaded from ENA using the accession code ERA30995399. All scripts necessary to reproduce the statistical analysis achieved in this manuscript are available (https://github.com/EmileFaure/Nickel_Omics). Tables summarizing quality-filtering and assembly steps statistics are available from the doi: 10.6084/m9.figshare.29127848.

Author contribution

ME, CH, NC, LM planned the campaign. NL, EF, DV and LM co-designed the study. NL, RZ, CA, MS, EF, YL collected samples and/or data. ME, CH, NC, LM, DV and NL acquired fundings. NL and EF wrote the manuscript draft. All co-authors interpreted and discussed the results and contributed to the revision of the manuscript draft.

Competing interests

The authors declare that they have no conflict of interest.

Acknowledgments

We would like to thank the captain and the crew of the R/V Akademik Tryoshnikov, and the chief scientist, the late David Walton for their support at sea. Special thanks go to members of the trace metal clean sampling team including Damien Cabanes, Roger Francois, Marion Fourquez, Samuel Jaccard, Julie Janssen, David Janssen, Maureen Soon and Gregory de Souza. This study was supported by ETH Zurich (through the grant 200021_184873 from the Swiss National Science Foundation), Projects 13 and 15 of the Antarctic Circumnavigation Expedition (funded by EPFL, Swiss Polar Institute and Ferring Pharmaceuticals) and the ANR French Research Foundation ANR-18-CE02-0024 (ACE ecogenomics project). Nolwenn Lemaitre has received funding from the European Union under the Marie Skłodowska-Curie grant agreement 101066172 (IsoMargin project). Views and opinions expressed are however those of the authors only and do not necessarily

https://doi.org/10.5194/egusphere-2025-6336
Preprint. Discussion started: 19 January 2026

reflect those of the European Union or the REA.A – Marie Sklodowska-Curie Actions & Support to Experts. Neither the European Union nor the granting authority can be held responsible for them.

References

Alonso-Sáez, L., Waller, A. S., Mende, D. R., Bakker, K., Farnelid, H., Yager, P. L., Lovejoy, C., Tremblay, J. É., Potvin, M., Heinrich, F., Estrada, M., Riemann, L., Bork, P., Pedrós-Alió, C., and Bertilssona, S.: Role for urea in nitrification by polar marine Archaea, Proc Natl Acad Sci U S A, 109, 17989–17994, https://doi.org/10.1073/pnas.1201914109, 2012.

Antoine, D., Thomalla, S., Berliner, D., Little, H., Moutier, W., Olivier-Morgan, A., Robinson, C., Ryan-Keogh, T., and Schuback, N.: Phytoplankton pigment concentrations of seawater sampled during the Antarctic Circumnavigation Expedition (ACE) during the Austral Summer of 2016/2017., https://doi.org/10.5281/ZENODO.3816726, 2020.

Aramaki, T., Blanc-Mathieu, R., Endo, H., Ohkubo, K., Kanehisa, M., Goto, S., and Ogata, H.: KofamKOALA: KEGG Ortholog assignment based on profile HMM and adaptive score threshold, Bioinformatics, 36, 2251–2252, https://doi.org/10.1093/bioinformatics/btz859, 2020.

Archer, C., Vance, D., Milne, A., and Lohan, M. C.: The oceanic biogeochemistry of nickel and its isotopes: New data from the South Atlantic and the Southern Ocean biogeochemical divide, Earth Planet Sci Lett, 535, 116118, https://doi.org/10.1016/j.epsl.2020.116118, 2020.

Benoit, G., Peterlongo, P., Mariadassou, M., Drezen, E., Schbath, S., Lavenier, D., and Lemaitre, C.: Multiple comparative metagenomics using multiset k-mer counting, PeerJ Comput Sci, 2016, 1–25, https://doi.org/10.7717/peerj-cs.94, 2016.

Bian, X., Yang, S. C., Raad, R. J., Odendahl, C. E., Lanning, N. T., Sieber, M., Huang, K. F., Fitzsimmons, J. N., Conway, T. M., and John, S. G.: Distribution and Cycling of Nickel and Nickel Isotopes in the Pacific Ocean, Geophys Res Lett, 51, e2024GL111115, https://doi.org/10.1029/2024GL111115, 2024.

Bruland, K. W.: Oceanographic distributions of cadmium, zinc, nickel, and copper in the North Pacific, Earth Planet Sci Lett, 47, 176–198, https://doi.org/10.1016/0012-821X(80)90035-7, 1980.

Cameron, V. and Vance, D.: Heavy nickel isotope compositions in rivers and the oceans, Geochim Cosmochim Acta, 128, 195–211, https://doi.org/10.1016/j.gca.2013.12.007, 2014.

Chen, C.-C., Rodriguez, I. B., Chen, Y.-L. L., Zehr, J. P., Chen, Y.-R., Hsu, S.-T. D., Yang, S.-C., and Ho, T.-Y.: Nickel superoxide dismutase protects nitrogen fixation in Trichodesmium, Limnol Oceanogr Lett, 7, 363–371, https://doi.org/10.1002/lol2.10263, 2022.

Cutter, G., Casciotti, K., Croot, P., Geibert, W., Heimbürger, L.-E., Lohan, M., Planquette, H., and Van De Flierdt, T.: Sampling and the sample-handling protocoles for GEOTRACES cruises, 1–178 pp., https://doi.org/http://www.geotraces.org/science/intercalibration/222-sampling-and-sample-handling-protocols-for-geotraces-cruises, 2017.

https://doi.org/10.5194/egusphere-2025-6336
Preprint. Discussion started: 19 January 2026

Doré, H., Guyet, U., Leconte, J., Farrant, G. K., Alric, B., Ratin, M., Ostrowski, M., Ferrieux, M., Brillet-Guéguen, L., Hoebeke, M., Siltanen, J., Le Corguillé, G., Corre, E., Wincker, P., Scanlan, D. J., Eveillard, D., Partensky, F., and Garczarek, L.: Differential global distribution of marine picocyanobacteria gene clusters reveals distinct niche-related adaptive strategies, ISME Journal, 17, 720–732, https://doi.org/10.1038/s41396-023-01386-0, 2023.

Dupont, C. L., Neupane, K., Shearer, J., and Palenik, B.: Diversity, function and evolution of genes coding for putative Ni-containing superoxide dismutases, Environ Microbiol, 10, 1831–1843, https://doi.org/10.1111/j.1462-2920.2008.01604.x, 2008a.

Dupont, C. L., Barbeau, K., and Palenik, B.: Ni uptake and limitation in marine Synechococcus strains., Appl Environ Microbiol, 74, 23–31, https://doi.org/10.1128/AEM.01007-07, 2008b.

Dupont, C. L., Buck, K. N., Palenik, B., and Barbeau, K.: Nickel utilization in phytoplankton assemblages from contrasting oceanic regimes, Deep-Sea Research Part I, 57, 553–566, https://doi.org/10.1016/j.dsr.2009.12.014, 2010.

Egleston, E. S. and Morel, M. M.: Nickel limitation and zinc toxicity in a urea-grown diatom, Limnol Oceanogr, 53, 2462–2471, https://doi.org/https://doi.org/10.4319/lo.2008.53.6.2462, 2008.

Eren, A. M., Vineis, J. H., Morrison, H. G., and Sogin, M. L.: A Filtering Method to Generate High Quality Short Reads Using Illumina Paired-End Technology, PLoS One, 8, e66643, https://doi.org/10.1371/journal.pone.0066643, 2013.

Eren, A. M., Esen, O. C., Quince, C., Vineis, J. H., Morrison, H. G., Sogin, M. L., and Delmont, T. O.: Anvi'o: An advanced analysis and visualization platformfor 'omics data, PeerJ, 3, 1–29, https://doi.org/10.7717/peerj.1319, 2015.

Faure, E., Pommellec, J., Noel, C., Cormier, A., Delpech, L.-M., Eren, M., Fernandez-Guerra, A., Vanni, C., Fourquez, M., Houssais, M.-N., Silva, C. Da, Gavory, F., Perdereau, A., Labadie, K., Wincker, P., Poulain, J., Hassler, C., Lin, Y., Cassar, N., and Maignien, L.: Water mass specific genes dominate the Southern Ocean microbiome, Res Sq, 1–25, https://doi.org/10.21203/rs.3.rs-5608865/v1, 2025.

Fourquez, M., Janssen, D. J., Conway, T. M., Cabanes, D., Ellwood, M. J., Sieber, M., Trimborn, S., and Hassler, C.: Chasing iron bioavailability in the Southern Ocean: Insights from Phaeocystis antarctica and iron speciation, Sci Adv, 9, eadf9696, https://doi.org/10.1126/sciadv.adf9696, 2023.

GEOTRACES Intermediate Data Product Group: The GEOTRACES GEOTRACES Intermediate Data Product 2021 (IDP2021), NERC EDS British Oceanographic Data Centre NOC., https://doi.org/doi:10.5285/cf2d9ba9-d51d-3b7c-e053-8486abc0f5fd, 2021.

Greening, C., Biswas, A., Carere, C. R., Jackson, C. J., Taylor, M. C., Stott, M. B., Cook, G. M., and Morales, S. E.: Genomic and metagenomic surveys of hydrogenase distribution indicate H 2 is a widely utilised energy source for microbial growth and survival, ISME Journal, 10, 761–777, https://doi.org/10.1038/ismej.2015.153, 2016.

Gueguen, B. and Rouxel, O.: The Nickel isotope composition of the authigenic sink and the diagenetic flux in modern oceans, Chem Geol, 563, 120050, https://doi.org/10.1016/j.chemgeo.2020.120050, 2021.

https://doi.org/10.5194/egusphere-2025-6336
Preprint. Discussion started: 19 January 2026

Gueguen, B., Rouxel, O., Ponzevera, E., Bekker, A., and Fouquet, Y.: Nickel Isotope Variations in Terrestrial Silicate Rocks and Geological Reference Materials Measured by MC-ICP-MS, Geostand Geoanal Res, 37, 297–317, https://doi.org/10.1111/j.1751-908X.2013.00209.x, 2013.

Ho, T.: Nickel limitation of nitrogen fixation in Trichodesmium, Limnol Oceanogr, 58, 112–120, https://doi.org/10.4319/lo.2013.58.1.0112, 2013.

Huerta-Cepas, J., Forslund, K., Coelho, L. P., Szklarczyk, D., Jensen, L. J., Von Mering, C., and Bork, P.: Fast genome-wide functional annotation through orthology assignment by eggNOG-mapper, Mol Biol Evol, 34, 2115–2122, https://doi.org/10.1093/molbev/msx148, 2017.

Hyatt, D., Chen, G.-L., Locascio, P. F., Land, M. L., Larimer, F. W., and Hauser, L. J.: Prodigal: prokaryotic gene recognition and translation initiation site identification, BMC Bioinformatics, 11, 1–11, https://doi.org/http://www.biomedcentral.com/1471-2105/11/119, 2010.

Janssen, D. J., Sieber, M., Ellwood, M. J., Conway, T. M., Barrett, P. M., Chen, X., de Souza, G. F., Hassler, C. S., and Jaccard, S. L.: Trace metal and nutrient dynamics across broad biogeochemical gradients in the Indian and Pacific sectors of the Southern Ocean, Mar Chem, 221, 103773, https://doi.org/10.1016/j.marchem.2020.103773, 2020.

John, S. G., Kelly, R. L., Bian, X., Fu, F., Smith, M. I., Lanning, N. T., Liang, H., Pasquier, B., Seelen, E. A., Holzer, M., Wasylenki, L., Conway, T. M., Fitzsimmons, J. N., Hutchins, D. A., and Yang, S.: The biogeochemical balance of oceanic nickel cycling, Nat Geosci, 15, 906–912, https://doi.org/10.1038/s41561-022-01045-7, 2022.

John, S. G., Liang, H., Pasquier, B., Holzer, M., and Silva, S.: Biogeochemical fluxes of nickel in the global oceans inferred from a diagnostic model, Global Biogeochem Cycles, 38, https://doi.org/10.1029/2023GB008018, 2024.

Langmead, B. and Salzberg, S. L.: Fast gapped-read alignment with Bowtie 2, Nat Methods, 9, 357–359, https://doi.org/10.1038/nmeth.1923, 2012.

Lemaitre, N., Du, J., de Souza, G. F., Archer, C., and Vance, D.: The essential bioactive role of nickel in the oceans : Evidence from nickel isotopes, Earth Planet Sci Lett, 584, 117513, https://doi.org/10.1016/j.epsl.2022.117513, 2022.

Levine, N. M. and Leles, S. G.: Marine plankton metabolisms revealed, Nat Microbiol, 6, 147–148, https://doi.org/10.1038/s41564-020-00856-x, 2021.

Li, D., Liu, C. M., Luo, R., Sadakane, K., and Lam, T. W.: MEGAHIT: An ultra-fast single-node solution for large and complex metagenomics assembly via succinct de Bruijn graph, Bioinformatics, 31, 1674–1676, https://doi.org/10.1093/bioinformatics/btv033, 2015.

Li, H., Tuo, S., Lu, M., and Ho, T.: The effects of Ni availability on H2 production and N2 fixation in a model unicellular diazotroph: The expression of hydrogenase and nitrogenase, Limnol Oceanogr, 9999, 1–11, https://doi.org/10.1002/lno.12151, 2022.

Li, W. and Godzik, A.: Cd-hit: A fast program for clustering and comparing large sets of protein or nucleotide sequences, Bioinformatics, 22, 1658–1659, https://doi.org/10.1093/bioinformatics/btl158, 2006.

https://doi.org/10.5194/egusphere-2025-6336
Preprint. Discussion started: 19 January 2026

Liu, Y., Debeljak, P., Rembauville, M., Blain, S., and Obernosterer, I.: Diatoms shape the biogeography of heterotrophic prokaryotes in early spring in the Southern Ocean, Environ Microbiol, 21, 1452–1465, https://doi.org/10.1111/1462-2920.14579, 2019.

Love, M. I., Huber, W., and Anders, S.: Moderated estimation of fold change and dispersion for RNA-seq data with DESeq2, Genome Biol, 15, 1–21, https://doi.org/10.1186/s13059-014-0550-8, 2014.

Lu, J., Rincon, N., Wood, D. E., Breitwieser, F. P., Pockrandt, C., Langmead, B., Salzberg, S. L., and Steinegger, M.: Metagenome analysis using the Kraken software suite, Nat Protoc, 17, 2815–2839, https://doi.org/10.1038/s41596-022-00738-y, 2022.

Mackey, D. J., O'Sullivan, J. E., Watson, R. J., and Dal Pont, G.: Trace metals in the Western Pacific: temporal and spatial variability in the concentrations of Cd, Cu, Mn and Ni, Deep Sea Res 1 Oceanogr Res Pap, 49, 2241–2259, https://doi.org/10.1016/S0967-0637(02)00124-3, 2002.

Middag, R., Baar, H. J. W. De, Bruland, K. W., and van Heuven, S. M. A. C.: The distribution of nickel in the west-Atlantic Ocean, its relationship with phosphate and a comparison to cadmium and zinc, Front Mar Sci, 7, 1–17, https://doi.org/10.3389/fmars.2020.00105, 2020.

Morel, F. M. M., Lam, P. J., and Saito, M. A.: Trace metal substitution in marine phytoplankton, Annu Rev Earth Planet Sci, 48, 491–517, https://doi.org/10.1146/annurev-earth-053018-060108, 2020.

Oksanen, J., Simpson, G. L., Blanchet, G., Kindt, R., Legendre, P., Minchin, P. R., O'Hara, R. B., Solymos, P., Henrey, M., Stevens, H., Szoecs, E., Wagner, H., Barbour, M., Bedward, M., Bolker, B., Borcard, D., Carvalho, G., Chirico, M., De Caceres, M., Durand, S., Beatriz, H., Evangelista, A., Firtz-John, R., Friendly, M., Furneaux, B., Hannigan, G., Hill, M. O., Lahti, L., McGlinn, D., Ouellette, M.-H., Ribeiro Cunha, E., Smith, T., Stier, A., Ter Braak, C. J. F., and Weedon, J.: vegan: Community Ecology Package. R package version 2.6-2, 2022.

Orsi, A. H., Whitworth III, T., and Nowlin, W. D.: On the meridional extent and fronts of the Antarctic Circumpolar Current, Deep-Sea Research I, 42, 641–673, 1995.

Parks, D. H., Chuvochina, M., Rinke, C., Mussig, A. J., Chaumeil, P. A., and Hugenholtz, P.: GTDB: An ongoing census of bacterial and archaeal diversity through a phylogenetically consistent, rank normalized and complete genome-based taxonomy, Nucleic Acids Res, 50, D785–D794, https://doi.org/10.1093/nar/gkab776, 2022.

Price, N. M. and Morel, F. M. M.: Colimitation of phytoplankton growth by nickel and nitrogen, Limnol Oceanogr, 36, 1071–1077, https://doi.org/10.4319/lo.1991.36.6.1071, 1991.

Ragsdale, S. W.: Nickel-based enzyme systems, Journal of biological chemistry, 284, 18571–18575, https://doi.org/10.1074/jbc.R900020200, 2009.

Rickli, J., Janssen, D. J., Hassler, C., Ellwood, M. J., and Jaccard, S. L.: Chromium biogeochemistry and stable isotope distribution in the Southern Ocean, Geochim Cosmochim Acta, 262, 188–206, https://doi.org/10.1016/j.gca.2019.07.033, 2019.

https://doi.org/10.5194/egusphere-2025-6336
Preprint. Discussion started: 19 January 2026

Robinson, C. M., Huot, Y., Schuback, N., Ryan-Keogh, T. J., Thomalla, S. J., and Antoine, D.: High latitude Southern Ocean phytoplankton have distinctive bio-optical properties, Opt Express, 29, 21084–21112, https://doi.org/10.1364/oe.426737, 2021.

Sarmiento, J. L., Gruber, N., Brzezinski, M. a, and Dunne, J. P.: High-latitude controls of thermocline nutrients and low latitude biological productivity., Nature, 427, 56–60, https://doi.org/10.1038/nature10605, 2004.

Sclater, F. R., Boyle, E., and Edmond, J. M.: On the marine geochemistry of nickel, Earth Planet Sci Lett, 31, 119–128, https://doi.org/https://doi.org/10.1016/0012-821X(76)90103-5, 1976.

Shaffer, J. P., Nothias, L. F., Thompson, L. R., Sanders, J. G., Salido, R. A., Couvillion, S. P., Brejnrod, A. D., Lejzerowicz, F., Haiminen, N., Huang, S., Lutz, H. L., Zhu, Q., Martino, C., Morton, J. T., Karthikeyan, S., Nothias-Esposito, M., Dührkop, K., Böcker, S., Kim, H. W., Aksenov, A. A., Bittremieux, W., Minich, J. J., Marotz, C., Bryant, M. K. M., Sanders, K., Schwartz, T., Humphrey, G., Vásquez-Baeza, Y., Tripathi, A., Parida, L., Carrieri, A. P., Beck, K. L., Das, P., González, A., McDonald, D., Ladau, J., Karst, S. M., Albertsen, M., Ackermann, G., DeReus, J., Thomas, T., Petras, D., Shade, A., Stegen, J., Song, S. J., Metz, T. O., Swafford, A. D., Dorrestein, P. C., Jansson, J. K., Gilbert, J. A., Knight, R., Angenant, L. T., Berry, A. M., Bittleston, L. S., Bowen, J. L., Chavarría, M., Cowan, D. A., Distel, D., Girguis, P. R., Huerta-Cepas, J., Jensen, P. R., Jiang, L., King, G. M., Lavrinienko, A., MacRae-Crerar, A., Makhalanyane, T. P., Mappes, T., Marzinelli, E. M., Mayer, G., McMahon, K. D., Metcalf, J. L., Miyake, S., Mousseau, T. A., Murillo-Cruz, C., Myrold, D., Palenik, B., Pinto-Tomás, A. A., Porazinska, D. L., Ramond, J. B., Rowher, F., RoyChowdhury, T., Sandin, S. A., Schmidt, S. K., Seedorf, H., Shade, A., Shipway, J. R., Smith, J. E., Stegen, J., Stewart, F. J., Tait, K., Thomas, T., Tucker, Y., U'Ren, J. M., Watts, P. C., Webster, N. S., Zaneveld, J. R., and Zhang, S.: Standardized multi-omics of Earth's microbiomes reveals microbial and metabolite diversity, Nat Microbiol, 7, 2128–2150, https://doi.org/10.1038/s41564-022-01266-x, 2022.

Sieber, M., Conway, T. M., de Souza, G. F., Hassler, C. S., Ellwood, M. J., and Vance, D.: High-resolution Cd isotope systematics in multiple zones of the Southern Ocean from the Antarctic Circumnavigation Expedition, Earth Planet Sci Lett, 527, 115799, https://doi.org/10.1016/j.epsl.2019.115799, 2019.

Sieber, M., Conway, T. M., de Souza, G. F., Hassler, C. S., Ellwood, M. J., and Vance, D.: Cycling of zinc and its isotopes across multiple zones of the Southern Ocean: Insights from the Antarctic Circumnavigation Expedition, Geochim Cosmochim Acta, 268, 310–324, https://doi.org/10.1016/j.gca.2019.09.039, 2020.

Sieber, M., Conway, T. M., de Souza, G. F., Hassler, C. S., Ellwood, M. J., and Vance, D.: Isotopic fingerprinting of biogeochemical processes and iron sources in the iron-limited surface Southern Ocean, Earth Planet Sci Lett, 567, 116967, https://doi.org/10.1016/j.epsl.2021.116967, 2021.

Sohrin, Y., Urushihara, S., Nakatsuka, S., Kono, T., Higo, E., Minami, T., Norisuye, K., and Umetani, S.: Multielemental determination of GEOTRACES key trace metals in seawater by ICPMS after preconcentration using an ethylenediaminetriacetic acid chelating resin, Anal Chem, 80, 6267–6273, https://doi.org/10.1021/ac800500f, 2008.

Stanke, M., Steinkamp, R., Waack, S., and Morgenstern, B.: AUGUSTUS: A web server for gene finding in eukaryotes, Nucleic Acids Res, 32, 309–312, https://doi.org/10.1093/nar/gkh379, 2004.

https://doi.org/10.5194/egusphere-2025-6336
Preprint. Discussion started: 19 January 2026

Sunagawa, S., Coelho, L. P., Chaffron, S., Kultima, J. R., Labadie, K., Salazar, G., Djahanschiri, B., Zeller, G., Mende, D. R., Alberti, A., Cornejo-Castillo, F. M., Costea, P. I., Cruaud, C., D'Ovidio, F., Engelen, S., Ferrera, I., Gasol, J. M., Guidi, L., Hildebrand, F., Kokoszka, F., Lepoivre, C., Lima-Mendez, G., Poulain, J., Poulos, B. T., Royo-Llonch, M., Sarmento, H., Vieira-Silva, S., Dimier, C., Picheral, M., Searson, S., Kandels-Lewis, S., Pesant, S., Speich, S., Stemmann, L., Sullivan, M. B., Weissenbach, J., Wincker, P., Karsenti, E., Raes, J., Acinas, S. G., and Bork, P.: Structure and function of the global ocean microbiome, Science (1979), 348, 1–10, https://doi.org/10.1126/science.1261359, 2015.

Sutherland, K. M., Ward, L. M., Colombero, C. R., and Johnston, D. T.: Inter-domain horizontal gene transfer of nickel-binding superoxide dismutase, Geobiology, 19, 450–459, https://doi.org/10.1111/gbi.12448, 2021.

Suzek, B. E., Wang, Y., Huang, H., McGarvey, P. B., Wu, C. H., and UniProt Consortium, the: UniRef clusters: A comprehensive and scalable alternative for improving sequence similarity searches, Bioinformatics, 31, 926–932, https://doi.org/10.1093/bioinformatics/btu739, 2015.

Takano, S., Tanimizu, M., Hirata, T., Shin, K.-C., Fukami, Y., Suzuki, K., and Sohrin, Y.: A simple and rapid method for isotopic analysis of nickel, copper, and zinc in seawater using chelating extraction and anion exchange, Anal Chim Acta, 967, 1–11, https://doi.org/10.1016/j.aca.2017.03.010, 2017.

Teeling, H., Fuchs, B. M., Becher, D., Klockow, C., Gardebrecht, A., Bennke, C. M., Kassabgy, M., Huang, S., Mann, A. J., Waldmann, J., Weber, M., Klindworth, A., Otto, A., Lange, J., Bernhardt, J., Reinsch, C., Hecker, M., Peplie, J., Bockelmann, F. D., Callies, U., Gerdts, G., Wichels, A., Wiltshire, K. H., Glöckner, F. O., Schweder, T., and Amann, R.: Substrate-controlled succession of marine bacterioplankton populations induced by a phytoplankton bloom, Science (1979), 336, 608–611, https://doi.org/10.1126/science.1218344, 2012.

Tortell, P. D., Maldonado, M. T., and Price, N. M.: The role of heterotrophic bacteria in iron-limited ocean ecosystems, https://doi.org/10.1038/383330a0, 1996.

Tuo, S., Rodriguez, I. B., and Ho, T.: H2 accumulation and N2 fixation variation by Ni limitation in Cyanothece, Limnol Oceanogr, 65, 377–386, https://doi.org/10.1002/lno.11305, 2020.

Vanni, C., Schechter, M. S., Acinas, S. G., Barberán, A., Buttigieg, P. L., Casamayor, E. O., Delmont, T. O., Duarte, C. M., Eren, A. M., Finn, R. D., Kottmann, R., Mitchell, A., Sanchez, P., Siren, K., Steinegger, M., Glöckner, F. O., and Fernandez-Guerra, A.: Unifying the known and unknown microbial coding sequence space, Elife, 11, 1–60, https://doi.org/10.7554/eLife.67667, 2022.

de Vargas, C., Audic, S., Henry, N., Decelle, J., Mahé, F., Logares, R., Lara, E., Berney, C., Le Bescot, N., Probert, I., Carmichael, M., Poulain, J., Romac, S., Colin, S., Aury, J.-M., Bittner, L., Chaffron, S., Dunthorn, M., Engelen, S., Morard, R., Mulot, M., Scalco, E., Siano, R., Vincent, F., Zingone, A., Dimier, C., Picheral, M., Wincker, P., and Karsenti, E.: Eukaryotic plankton diversity in the sunlit ocean, Science (1979), 348, 1–12, https://doi.org/10.1126/science.1261605, 2015.

Vernette, C., Lecubin, J., Sánchez, P., Acinas, S. G., Babin, M., Bork, P., Boss, E., Bowler, C., Cochrane, G., De Vargas, C., Gorsky, G., Guidi, L., Grimsley, N., Hingamp1, P., Iudicone, D., Jaillon, O., Kandels-Lewis, S., Karp-Boss, L., Karsenti, E., Not, F., Ogata, H., Poulton, N., Pesant, S., Sardet, C., Speich, S., Stemmann, L., Sullivan, M. B., Sunagawa, S., Wincker, P.,

https://doi.org/10.5194/egusphere-2025-6336
Preprint. Discussion started: 19 January 2026

Sunagawa, S., Delmont, T. O., Pelletier, E., Pelletier, E., Hingamp, P., and Lescot, M.: The Ocean Gene Atlas v2.0: online exploration of the biogeography and phylogeny of plankton genes, Nucleic Acids Res, 50, W516–W526, https://doi.org/10.1093/nar/gkac420, 2022.

Wang, R. M., Archer, C., Bowie, A. R., and Vance, D.: Zinc and nickel isotopes in seawater from the Indian Sector of the Southern Ocean: The impact of natural iron fertilization versus Southern Ocean hydrography and biogeochemistry, Chem Geol, 511, 452–464, https://doi.org/10.1016/j.chemgeo.2018.09.010, 2019.

Wang, S. J. and Wasylenki, L. E.: Experimental constraints on reconstruction of Archean seawater Ni isotopic composition from banded iron formations, Geochim Cosmochim Acta, 206, 137–150, https://doi.org/10.1016/j.gca.2017.02.023, 2017.

White, R. A., Callister, S. J., Moore, R. J., Baker, E. S., and Jansson, J. K.: The past, present and future of microbiome analyses, https://doi.org/10.1038/nprot.2016.148, 1 November 2016.

Yang, S., Kelly, R. L., Bian, X., Conway, T. M., Huang, K., Ho, T., Neibauer, J. A., Keil, R. G., Moffett, J. W., and John, S. G.: Lack of redox cycling for nickel in the water column of the Eastern tropical north pacific oxygen deficient zone : Insight from dissolved and particulate nickel isotopes, Geochim Cosmochim Acta, 309, 235–250, https://doi.org/10.1016/j.gca.2021.07.004, 2021.

Yang, S. C., Hawco, N. J., Pinedo-González, P., Bian, X., Huang, K.-F., Zhang, R., and John, S. G.: A new purification method for Ni and Cu stable isotopes in seawater provides evidence for widespread Ni isotope fractionation by phytoplankton in the North Pacific, Chem Geol, 547, 119662, https://doi.org/10.1016/j.chemgeo.2020.119662, 2020.

https://doi.org/10.5194/egusphere-2025-6336
Preprint. Discussion started: 19 January 2026

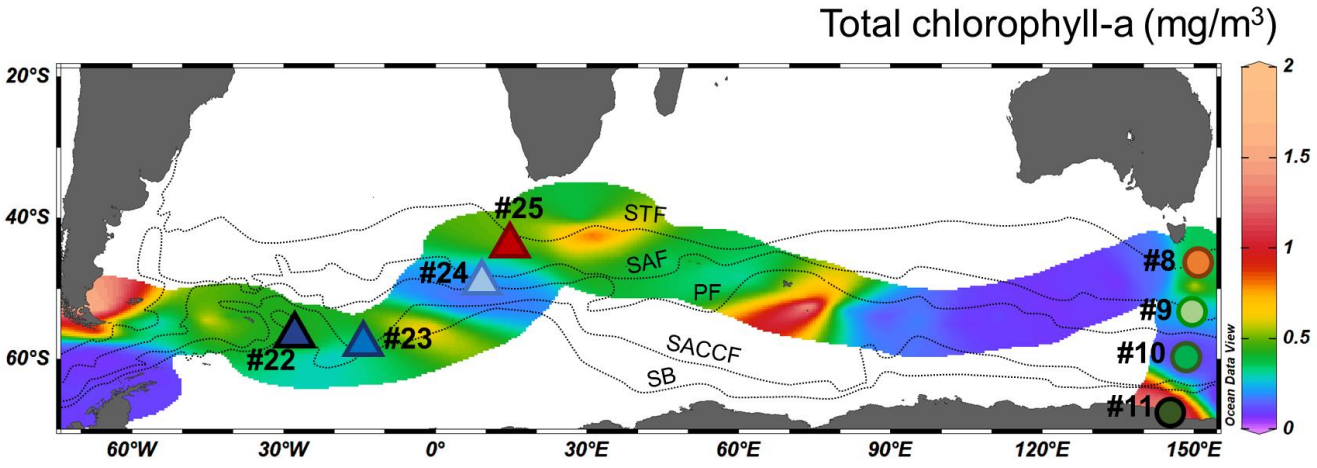

725

Figure 1: Location of the sampling stations for Ni concentrations and isotopes during the ACE cruise, superimposed on a map of total surface chlorophyll-*a* concentrations from underway seawater samples (all small grey circles Antoine et al., 2020). Blue and green symbols denote high latitude stations, while red and orange symbols represent stations north of the Sub-Antarctic Front from Leg 2 between Tasmania and Antarctica (circle symbols) and from Leg 3 between Patagonia and South Africa (triangle symbols). 730 **The major fronts (Orsi et al., 1995) are represented by the dotted black lines: Sub-Tropical Front (STF), Sub-Antarctic Front (SAF), Polar Front (PF), Southern ACC Front (SAAC) and Southern Boundary (SB).**

https://doi.org/10.5194/egusphere-2025-6336
Preprint. Discussion started: 19 January 2026

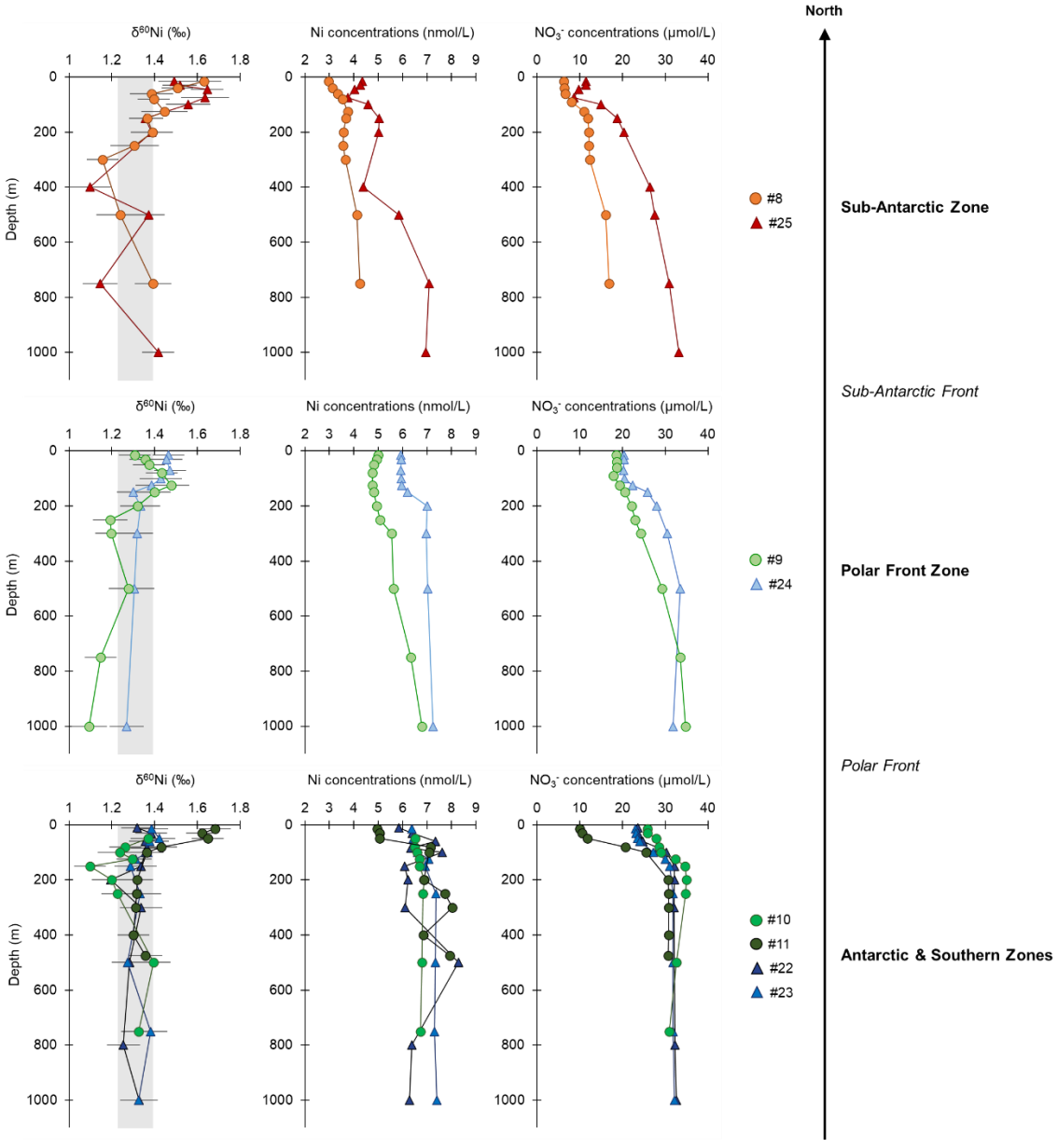

Figure 2: Depth profiles of dissolved Ni isotope compositions (δ^{60}Ni), Ni concentrations and nitrate (NO_3^-) concentrations (from Hassler and Ellwood, 2020) at eight stations of the ACE cruise. The top panels show data from the lower latitudes, in the Sub-Antarctic Zone. Below are panels from the high latitudes, in the Polar Front Zone and in the Antarctic and Southern Zones. The shaded grey band shows the average δ^{60}Ni in the deep ocean (1.34 ± 0.12 ‰, 2SD).

https://doi.org/10.5194/egusphere-2025-6336
Preprint. Discussion started: 19 January 2026

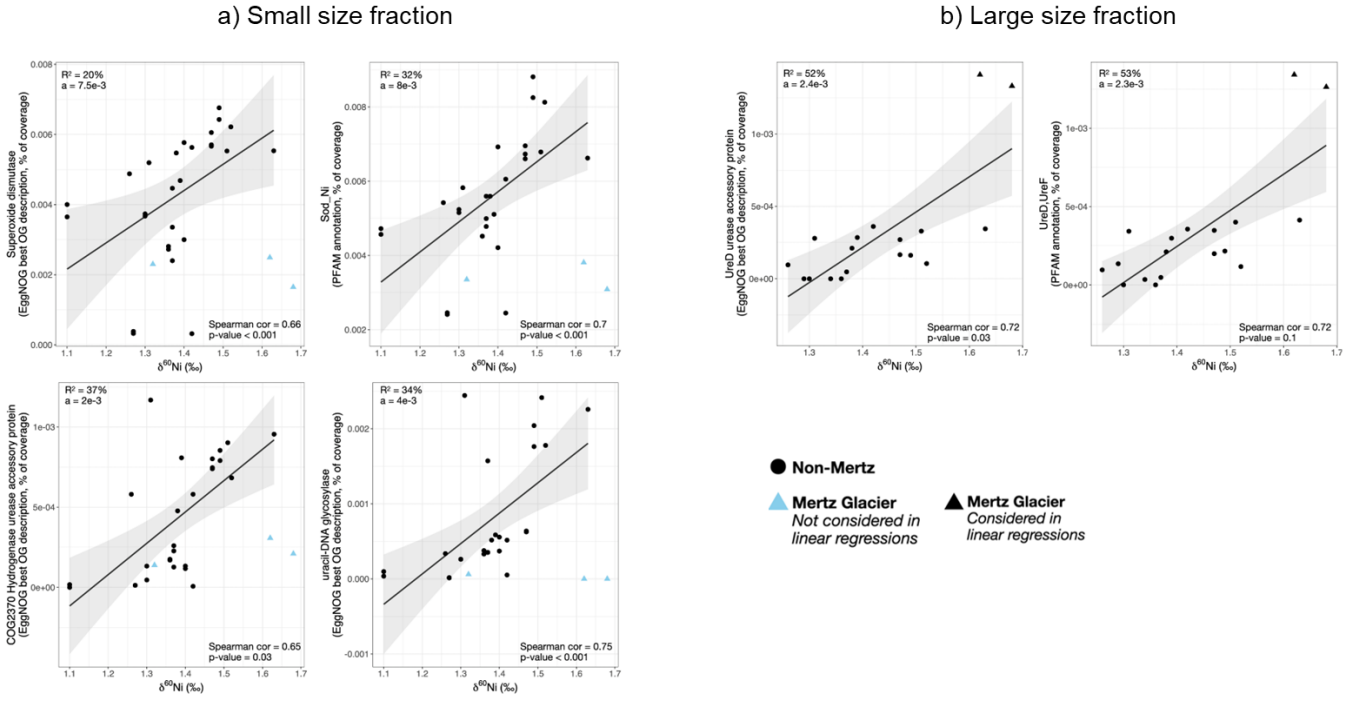

Figure 3: Relative metagenomic abundance (based on EggNOG best OG descriptions or PFAM annotations) as a function of δ^{60}Ni, along with a regression line and its 95% confidence interval, for a) the small size fraction (0.2 - 3 µm and 0.2 - 40 µm; left panels) and b) the large size fraction (3 – 200 µm; right panels). Light blue symbols were excluded from the computation of the linear regression lines, to illustrate how removing Mertz Glacier samples from the small size fraction leads to stronger relationships between some functions and δ^{60}Ni. Bonferroni-Hochberg corrected p-values are indicated on each graph (computed without Mertz samples in the small size fraction), along with Spearman coefficients (spearman cor). Adjusted R^2 and slope coefficients (a) of each linear regression are also shown in the top left.

https://doi.org/10.5194/egusphere-2025-6336
Preprint. Discussion started: 19 January 2026

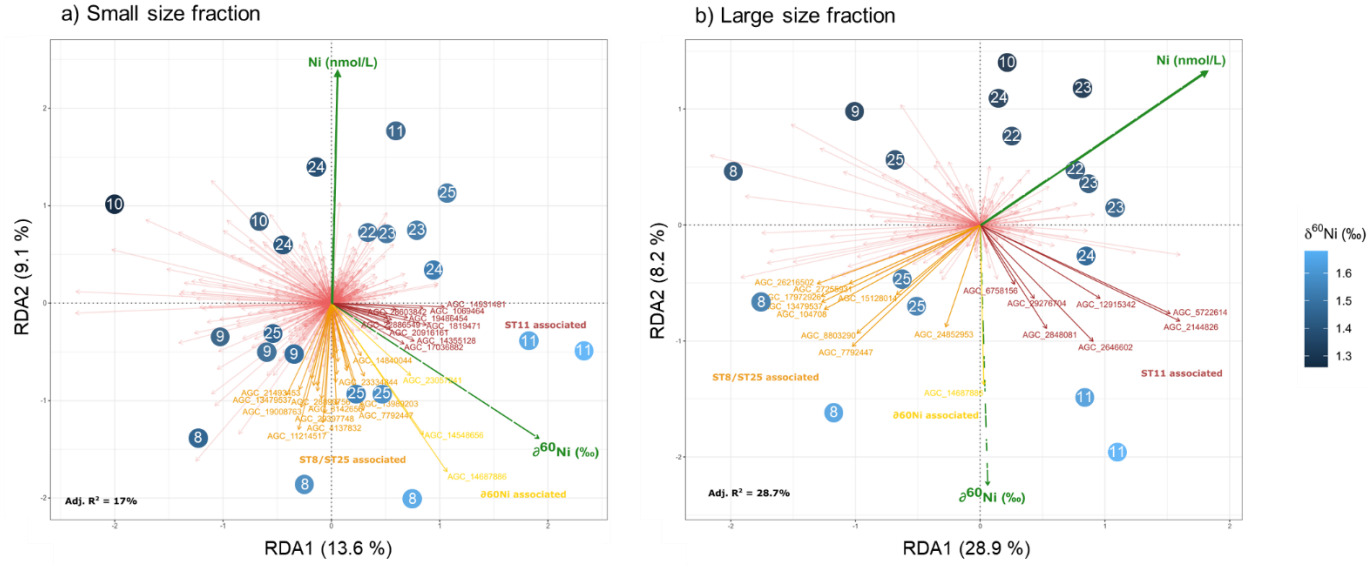

Figure 4: Redundancy analyses (RDA) on the rCLR-transformed abundance of AGNOSTOS gene clusters (AGC) and Ni distributions (concentrations and isotope compositions) for a) the small size fraction (0.2 - 3 µm and 0.2 - 40 µm; on the left side) and b) the large size fraction (3 - 200 µm; on the right side). Each plain arrow corresponds to a gene cluster. Light red arrows correspond to AGC unrelated to δ^{60}Ni, orange arrows to δ^{60}Ni-related AGC more abundant in stations 8 and 25, yellow arrows to δ^{60}Ni-related AGC well represented in all high-δ^{60}Ni stations, and dark red arrows to δ^{60}Ni-related AGC more abundant at station 11. Circles correspond to the different samples, with their station of origin written in white in the middle and a colour-coded for their δ^{60}Ni value. Taxonomic and functional annotations of these gene clusters are given in Tables 1 and S2.

https://doi.org/10.5194/egusphere-2025-6336
Preprint. Discussion started: 19 January 2026

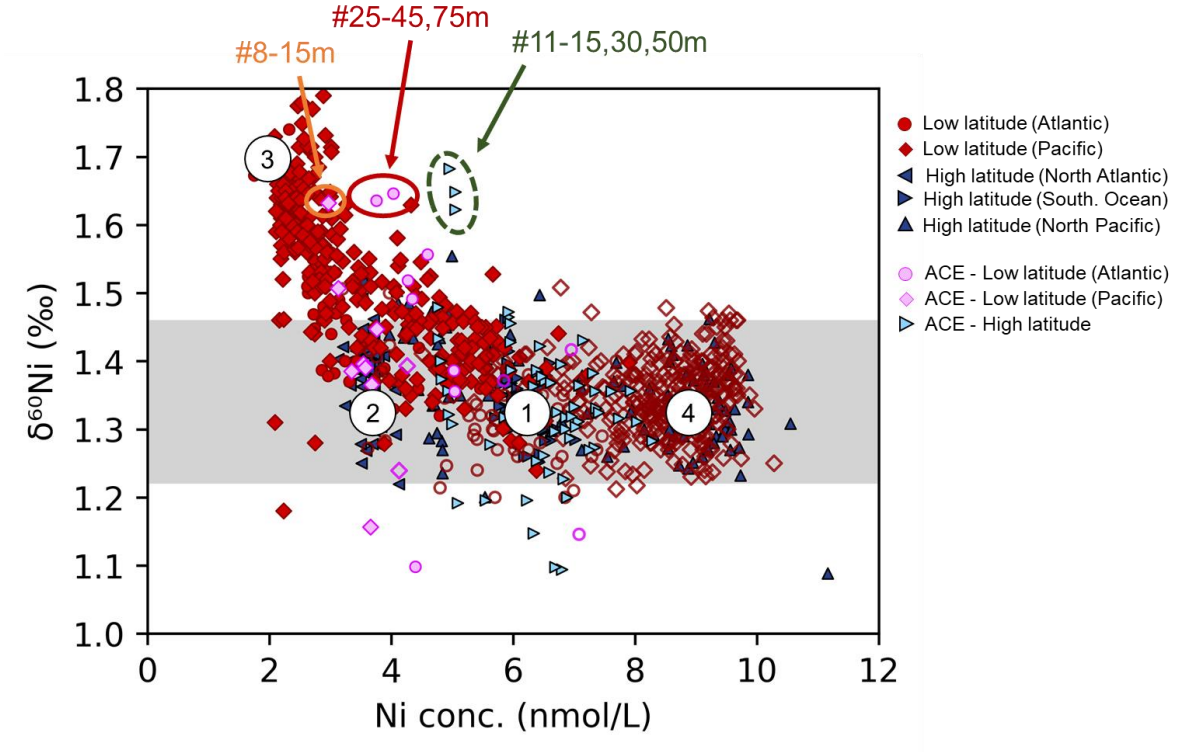

Figure 5: Comparison of the new ACE dataset with the dissolved Ni-δ^{60}Ni systematics of the global ocean (Cameron and Vance, 2014; Takano et al., 2017; Wang et al., 2019; Archer et al., 2020; Yang et al., 2020, 2021; Lemaitre et al., 2022; Bian et al., 2024; and this study). The shaded grey band shows the deep-ocean δ^{60}Ni value (see Figure 2).

https://doi.org/10.5194/egusphere-2025-6336
Preprint. Discussion started: 19 January 2026

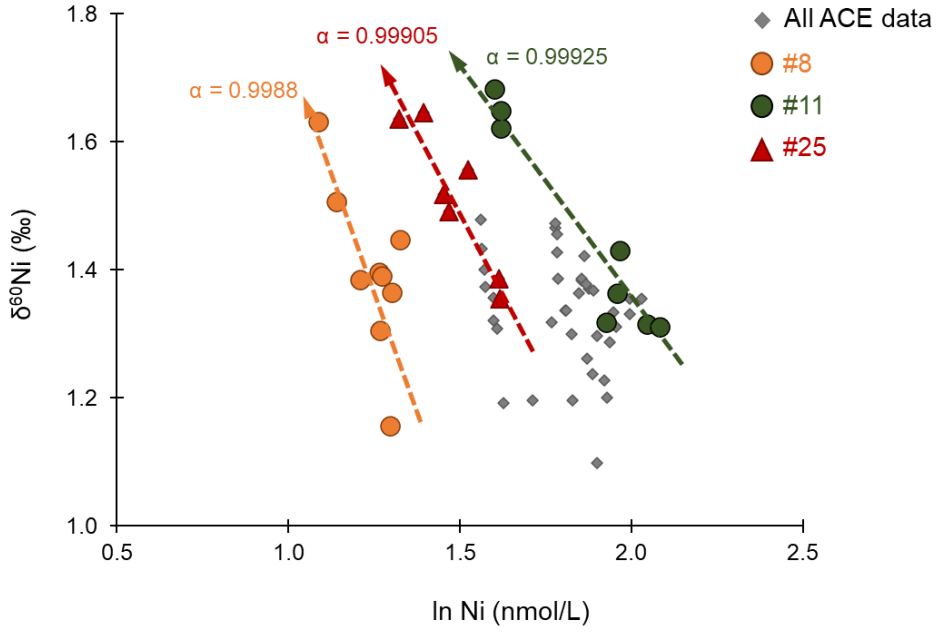

Figure 6: Ni isotope systematics in the upper 300 m of all ACE stations (in grey diamonds), and specifically at stations characterised by significantly heavy isotope compositions in surface waters (station 8 in orange circles, station 11 in dark green circles and station 25 in red triangles). The Rayleigh fractionation factors (α) were calculated using data from the upper 300 m. The arrows show modelled Rayleigh-type evolutions of the residual dissolved phase as Ni is removed from an initial pool ($\delta^{60}Ni_{initial}$ = 1.31‰) via a generalised uptake mechanism following the equation $R_{residual\ seawater} = R_{initial\ seawater} \times F^{\alpha-1}$, where $\alpha = R_{phytoplankton}/R_{seawater}$, $R=^{60}Ni/^{58}Ni$ and F is the fraction of the initial pool remaining.

https://doi.org/10.5194/egusphere-2025-6336
Preprint. Discussion started: 19 January 2026

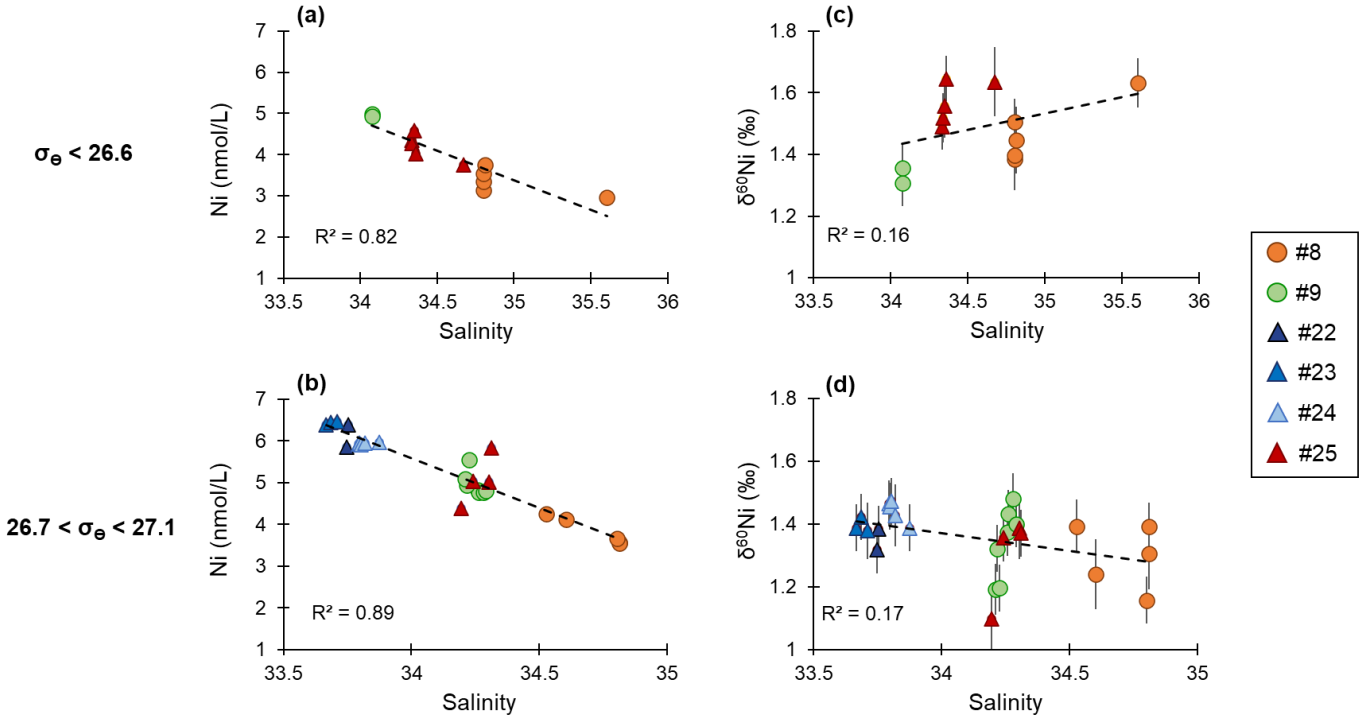

765

Figure 7: Ni concentrations (a and b) and Ni isotopes (c and d) versus salinity for surface waters (top panels; σ_Θ < 26.6) and for waters close to the SAMW isopycnals (bottom panels; 26.7 < σ_Θ < 27.1).

https://doi.org/10.5194/egusphere-2025-6336
Preprint. Discussion started: 19 January 2026

	Size fraction	AGNOSTOS gene cluster	Broad functional annotation	EggNOG based functional annotation	Taxonomic annotation (UniRef90 and GTDB)
δ^{60}Ni	small	AGC_14548656	urease	UreF	Roseobacteraceae, Rhodobacteraceae
	small	AGC_23057241	urease	UreD	Rhodobacteraceae
	small & large	AGC_14687886	urease	UreE_C,UreE_N	Roseobacteraceae, Rhodobacteraceae
Station 11	small	AGC_14355128	Ni-SOD	Sod_Ni	Polaribacter
	small	AGC_20916161	Ni-SOD	Sod_Ni	SAR92
	small	AGC_1069464	urease	UreE_C,UreE_N	Rhodobacteraceae
	large	AGC_2144826	urease	UreD,UreF	Bacillariaceae, Fragilariopsis cylindrus
	large	AGC_29276704	urease	Urease_alpha	Prymnesiaceae, Haptolina ericina
	large	AGC_12915342	urease	cobW,UreG	Naviculaceae, Craspedostauros australis
	large	AGC_6758156	urease	Urease_alpha,Urease_beta, Urease_gamma	Bacillariaceae; Fragilariopsis cylindrus
Stations 8 and 25	small	AGC_23334844	urease	cobW,UreG	Rhodobacteraceae, Roseobacteraceae
	small	AGC_2164110	Ni-SOD	Sod_Ni	Piscirickettsiaceae, Alteromonadaceae, Porticoccaceae
	small	AGC_17472745	NiFe hydrogenase	NiFeSe_Hases	Flavobacteriaceae
	small	AGC_24807388	urease	Urease_alpha,Urease_beta, Urease_gamma	Eukaryote
	small	AGC_8142656	urease	UreE_C,UreE_N	Synechococcus
	small	AGC_25996182	urease	UreD,UreF	Bathycoccaceae
	small	AGC_26196954	Ni-SOD	Sod_Ni	Phaeocystis
	small	AGC_29397748	Ni-SOD	Sod_Ni	Planctomycetaceae, Opitutaceae
	small & large	AGC_13479537	urease	Urease_beta,Urease_gamma	Proteobacteria
	large	AGC_8803290	urease	UreE_C,UreE_N	Rhodobacteraceae, Rhodospirillales, Alteromonadales
	large	AGC_104708	urease	cobW, urease accessory protein	Prasinoderma
	large	AGC_17972926	Ni-SOD	Sod_Ni	Bacillariaceae
	large	AGC_15128014	urease	Urease_alpha,Urease_beta, Urease_gamma	Phaeocystis
	large	AGC_27255931	urease	UreF	Proteobacteria, Synechococcus, Nitrospinae

Table 1: Functional and taxonomic annotations of selected AGNOSTOS gene clusters (AGC) emerging from the redundancy analyses as particularly linked to δ^{60}Ni (shown in yellow in Figure 4), station 11 (shown in red in Figure 4) and stations 8 and 25 (shown in orange in Figure 4). The selection of the AGC corresponds to those whose EggNOG best OG description and/or PFAM annotation was clearly related to Ni-dependent enzymes (i.e. not considering non-nickel SOD or ambiguous annotations related to urease like Uracyl-DNA glycosylase). Please, refer to Table S2 for the full functional and taxonomic annotations.